Gastroenterology 2020;159:956–968

Bile Acids Signal via TGR5 to Activate Intestinal Stem Cells and Epithelial Regeneration

Giovanni Sorrentino,[1] Alessia Perino,[1] Ece Yildiz,[1] Gaby El Alam,[1] Maroun Bou Sleiman,[1] Antimo Gioiello,[2] Roberto Pellicciari,[3] and Kristina Schoonjans[1]

[1]*Institute of Bioengineering, School of Life Sciences, École Polytechnique Fédérale de Lausanne, Lausanne, Switzerland;* [2]*Department of Pharmaceutical Sciences, University of Perugia, Perugia, Italy; and* [3]*TES Pharma, Perugia, Italy*

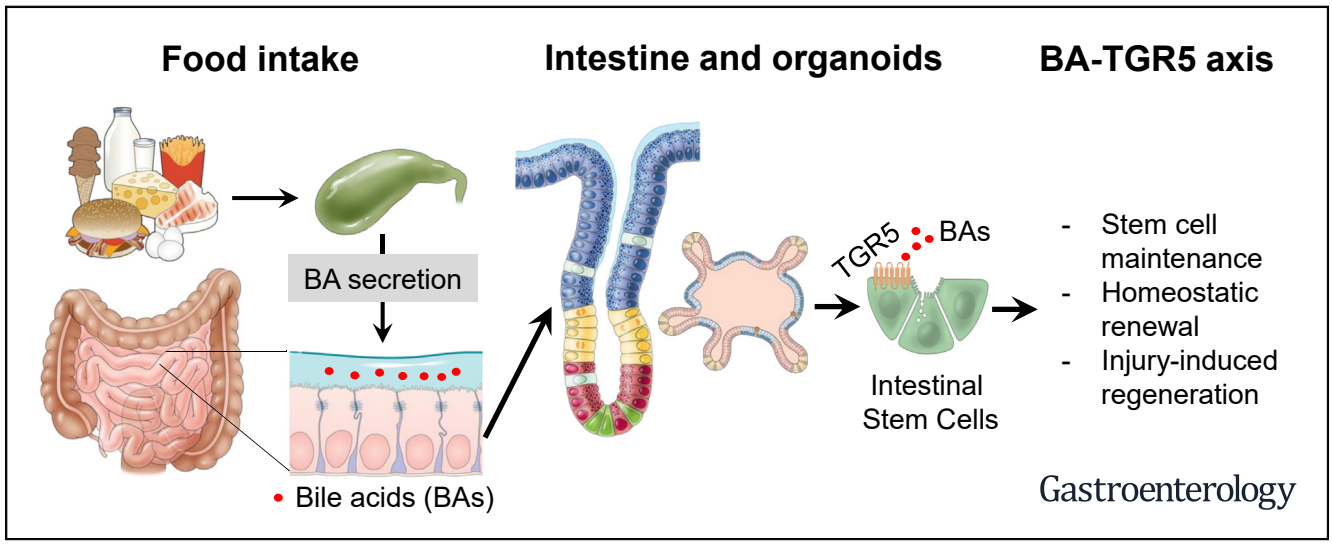

BACKGROUND & AIMS: Renewal and patterning of the intestinal epithelium is coordinated by intestinal stem cells (ISCs); dietary and metabolic factors provide signals to the niche that control ISC activity. Bile acids (BAs), metabolites in the gut, signal nutrient availability by activating the G protein-coupled bile acid receptor 1 (GPBAR1, also called TGR5). TGR5 is expressed in the intestinal epithelium, but it is not clear how its activation affects ISCs and regeneration of the intestinal epithelium. We studied the role of BAs and TGR5 in intestinal renewal, and regulation of ISC function in mice and intestinal organoids. **METHODS:** We derived intestinal organoids from wild-type mice and *Tgr5*$^{-/-}$ mice, incubated them with BAs or the TGR5 agonist INT-777, and monitored ISC function by morphologic analyses and colony-forming assays. We disrupted *Tgr5* specifically in *Lgr5*-positive ISCs in mice (*Tgr5*$^{ISC-/-}$ mice) and analyzed ISC number, proliferation, and differentiation by flow cytometry, immunofluorescence, and organoid assays. *Tgr5*$^{ISC-/-}$ mice were given cholecystokinin; we measured the effects of BA release into the intestinal lumen and on cell renewal. We induced colitis in *Tgr5*$^{ISC-/-}$ mice by administration of dextran sulfate sodium; disease severity was determined based on body weight, colon length, and histopathology analysis of colon biopsies. **RESULTS:** BAs and TGR5 agonists promoted growth of intestinal organoids. Administration of cholecystokinin to mice resulted in acute release of BAs into the intestinal lumen and increased proliferation of the intestinal epithelium. BAs and *Tgr5* expression in ISCs were required for homeostatic intestinal epithelial renewal and fate specification, and for regeneration after colitis induction. *Tgr5*$^{ISC-/-}$ mice developed more severe colitis than mice without *Tgr5* disruption in ISCs. ISCs incubated with INT-777 increased activation of yes-associated protein 1 (YAP1) and of its upstream regulator SRC. Inhibitors of YAP1 and SRC prevented organoid growth induced by TGR5 activation. **CONCLUSIONS:** BAs promote regeneration of the intestinal epithelium via activation of TGR5 in ISCs, resulting in activation of SRC and YAP and activation of their target genes. Release of endogenous BAs in the intestinal lumen is sufficient to promote ISC renewal and drives regeneration in response to injury.

Keywords: Secondary Bile Acids; IBD; GLP1; HFD; GPBAR1.

Abbreviations used in this paper: **BA, bile acid; CCK, cholecystokinin; CSC, cancer stem cell; DCA, deoxycholic acid; DSS, dextran sulfate sodium salt; FACS, fluorescence activated cell sorting; GFP, green fluorescent protein; HFD, high-fat diet; ISC, intestinal stem cell; LCA, lithocholic acid; PBS, phosphate-buffered saline; TA, transit amplifying; TGR5, Takeda G-coupled receptor 5; YAP, yes-associated protein.**

Most current article

0016-5085
https://doi.org/10.1053/j.gastro.2020.05.067

The epithelial surface of the intestine constitutes the largest barrier against the external environment. In most adult mammals, epithelial cells are renewed every 2 to 5 days to counteract intestinal damage and disruption of the barrier function.[1] Coordinated renewal and patterning of the intestinal epithelium is dictated by intestinal stem cells (ISCs), which are subject to tight regulation to fine-tune the balance between self-renewal and cell fate specification.[2] ISCs reside at the bottom of the intestinal crypts, where they are maintained in a multipotent state, and constantly generate transit amplifying (TA) progenitors. TA cells undergo a few cycles of division before migrating from the crypts to the villi to eventually differentiate into multiple intestinal epithelial cell lineages.[3] Diet has a profound impact on gut physiology; however, the nature and the mechanisms of this relationship are still poorly understood.[4–9] In this context, a number of dietary and metabolic factors have been recently found to act as niche signals to control ISC behavior.[4] Bile acids (BAs) are among the most abundant metabolites in the gut.[10] Shortly after food ingestion, BA levels rise in the intestinal lumen as a result of gallbladder contraction and intermingle with the food content to facilitate lipid digestion. BAs, however, are also able to act as versatile signaling molecules that relay nutrient availability to a physiological response.[11]

The BA-responsive membrane receptor, Takeda G-coupled receptor 5 (TGR5, aka GPBAR1), mediates several systemic processes and disruption of its function increases susceptibility to liver steatosis,[12] atherosclerosis,[13] diet-induced obesity,[14] and inflammation,[13,15] all features of the metabolic syndrome.[16] TGR5 is expressed throughout the entire gastrointestinal tract and also regulates many of the gut homeostatic functions of BAs, including gut hormone secretion,[17] gastrointestinal motility,[18] and local immune function.[19] Its expression is maintained in intestinal organoids where it triggers various intracellular signaling pathways on activation by secondary BAs.[20] Although its role is well established in particular subpopulations of the intestinal epithelium, such as in the enteroendocrine L-cells and immune regulatory cells, it is unknown whether the BA-TGR5 molecular axis coordinates intestinal cell renewal and specification through regulation of ISC function.

Using organotypic cultures and newly generated mouse models for TGR5, we demonstrate here that BAs control intestinal homeostasis by activating TGR5 specifically in the ISC pool. The BA-TGR5 axis regulates ISC number and function in vivo and critically controls homeostatic and damage-induced epithelial regeneration as well as ISC specification into enteroendocrine L-cells and Goblet cells. Mechanistically, we found that TGR5 operates through activation of the SRC/yes-associated protein (YAP) regenerative machinery to support intestinal cell proliferation and de novo ISC reconstitution. This unexpected role of BAs in orchestrating TGR5-mediated intestinal stemness provides novel mechanistic insights into the intimate relationship between dietary/metabolic cues and stem cell function, and could offer new treatment options for BA mimetics in intestinal regenerative therapies.

WHAT YOU NEED TO KNOW

BACKGROUND AND CONTEXT

Bile acids (BAs) signal nutrient availability by activating the G protein-coupled bile acid receptor 1 (GPBAR1, also called TGR5). TGR5 is expressed in the intestinal epithelium, but it is not clear how its activation affects intestinal stem cells and regeneration of the intestinal epithelium.

NEW FINDINGS

BAs promote regeneration of the intestinal epithelium via activation of TGR5 in intestinal stem cells, resulting in activation of SRC and YAP and activation of their target genes. Release of endogenous BAs in the intestinal lumen is sufficient for triggering intestinal stem cell renewal and proliferation and drives regeneration in response to injury.

LIMITATIONS

This study was performed in mice—further studies are needed with human tissues.

IMPACT

BAs or agents that activate TGR5 signaling might be developed for regeneration of the intestinal epithelium after injury.

Materials and Methods

Study Design

Mice were randomized into the different groups according to the genotype. The sample size was calculated on the basis of the known variability for each assay. A power analysis was performed to calculate the sample size for mouse experiments. Mice showing any sign of severity, predefined by the Veterinary Office of the Canton of Vaud, Switzerland were killed and excluded from the data analyses. These criteria were established before starting the experiments. Experiments in organoid models were performed at least 3 times. To focus on TGR5-specific signaling and avoid confounding effects of FXR activation, the selective TGR5 agonist INT-777 was used for some experiments instead of natural BAs. All experiments were performed in a nonblinded manner.

Mouse Strains

Lgr5-eGFP-IRES-CreERT2[21] reporter mice (*Lgr5-Tg* mice) were bred with mice carrying floxed alleles for the *Tgr5* gene ($Tgr5^{fl/fl}$ mice) to generate the *Lgr5-eGFP-IRES-CreERT2/*$Tgr5^{fl/fl}$ mice (*Lgr5-Tg/*$Tgr5^{fl/fl}$). In *Lgr5-Tg/*$Tgr5^{fl/fl}$ mice, tamoxifen was used to induce deletion of *Tgr5* in $Lgr5^{+}$ cells ($Tgr5^{ISC-/-}$ mice), whereas vehicle (corn oil) was used as control ($Tgr5^{ISC+/+}$ mice). For *Tgr5* deletion induction, 8- to 12-week-old male mice were given 2 mg of tamoxifen (oral gavage) for 5 consecutive days to ensure recombination in $Lgr5^{+}$ cells. To avoid possible off-target effects of tamoxifen and for experiments not requiring green fluorescent protein (GFP) expression in ISC, tamoxifen-exposed $Tgr5^{fl/fl}$ mice were used as controls of $Tgr5^{ISC\ -/-}$ mice. $Tgr5^{-/-}$ mice were described previously.[12]

Ethical Approval

All the mouse experiments were authorized by the Veterinary Office of the Canton of Vaud, Switzerland, under the license authorizations no. 3263 and 2257.2.

Proliferation Assay

Cell proliferation was assessed by EdU assay (Click-iT EdU Alexa Fluor 647, ThermoFisher,Waltham, MA) following manufacturer's instructions. Edu was resuspended in phosphate-buffered saline (PBS) and 200 μL of solution were injected intraperitoneally (50 μg per g of mouse weight). Cholecystokinin (CCK) was from Anawa (AS-22944; Zurich, Switzerland). For in vitro studies, EdU was added to the culture medium (10 μM) for 2 hours.

Organoid Cultures

Crypts were isolated from mice as described,[4] with minor modifications. Briefly, small intestines were flushed with PBS through a 20-mL syringe, opened longitudinally, and then washed with cold PBS by vigorous shaking. Villi were removed by carefully scraping the mucosa with a glass slide and then the tissue was minced to 1 mm^2 fragments. Intestinal samples were then incubated with EDTA 2 mM for 30 minutes at 4°C. Epithelium was detached by vigorous shaking. To enrich crypts, tissue suspension was filtered through 70-μm nylon mesh. Enriched crypts were washed once with cold PBS, counted, and plated into 20 μL Matrigel droplets (200 crypts per droplet). Crypt culture medium was Dulbecco's modified Eagle's medium/F12 medium (Invitrogen, Carlsbad, CA) supplemented with N2 (Invitrogen), B27 (Invitrogen), 1.25 mM N-acetylcysteine (Sigma-Aldrich, St Louis, MO), 1 $mg \cdot mL^{-1}$ RSPO1 (home-made), 20 $ng \cdot mL^{-1}$ epidermal growth factor (EGF) (PeproTech, Rocky Hill, NJ), 20 μM Y27632 (only for the first 2 days, Sigma-Aldrich) and 100 $ng \cdot mL^{-1}$ Noggin (home-made). Medium was replaced every 2 days. Secondary organoid generation assay was performed as previously described.[4] For ISC isolation, the crypts were dissociated into individual cells with 1× TrypLE express (Life Technologies, Carlsbad, CA) supplemented with DNaseI (Roche, Basel, Switzerland). According to GFP intensity, cells could be grouped into GFP^{hi} (ISCs) and GFP^{neg} (differentiated cells); 20×10^3 ISCs were embedded in 10 μL Matrigel droplets. ISC culture medium was the crypt culture medium containing JAG-1 (1 μM; Anaspec, Fremont, CA) and CHIR99021 (3 μM; Millipore, Bedford, MA). The surface area of organoids was measured microscopically by taking several random nonoverlapping photos of organoids (after 7 days in culture) using an inverted microscope. Each photo was analyzed using ImageJ software (National Institutes of Health, Bethesda, MD). Organoid perimeters for area measurements were defined manually. Organoids and ISCs were exposed every 2 days with lithocholic acid (LCA) (L6250; Sigma, St. Louis, MO), deoxycholic acid (DCA) (D2510; Sigma), BAmix (a crude bile extract that contains the sodium salts of taurocholic, glycocholic, deoxycholic, and cholic acids; S9875; Sigma), Verteporfin (SML0534; Sigma), Dasatinib (S1021; Selleckchem, Houston, TX), INT-777 (TES Pharma, Perugia, Italy), and 4-DAMP (SML0255; Sigma) at the indicated concentrations.

Fluorescence Activated Cell Sorting

Fluorescence activated cell sorting (FACS) was performed using a 4-laser MoFlo ASTRIOS EQ cell sorter from Beckman Coulter (Brea, CA). After gating out the doublets, the cell populations were subdivided accordingly to their GFP expression as GFP^{hi} and GFP^{neg}. The 488-nm laser was used to access the GFP expression (526/52).

Experimental Colitis and Regeneration Assay

Deletion of *Tgr5* was induced by oral gavage of tamoxifen (2 mg/body; dissolved in corn oil; Sigma; 1 gavage per day from day −7 to day −2 before the dextran sulfate sodium salt [DSS] initiation). Colitis was induced in mice (9 to 12 weeks old) by administration of 2.5% DSS (Sigma 42867) in drinking water. Daily changes in body weight were assessed. Mice were killed 7 days after DSS administration. To monitor epithelium regeneration, after 7 days from DSS initiation, DSS was changed with water for 3 days.

Histopathological Scoring

A European board-certified veterinary pathologist performed the histopathologic evaluation in a blinded fashion. The following parameters were identified: (1) severity of inflammation; (2) ulceration; (3) crypt damage. Histologic criteria for each parameter have been adopted and adapted.[22–24] The sum of the 3 parameter values was used to generate a "total histopathological score." Statistical analysis was performed using GraphPad Prism 7 Software (San Diego, CA). Data were compared by an unpaired 2-tailed *t test*. $P < .05$ was considered significant.

Statistical Analysis and Sample Information

Statistically significant differences between the means of 2 groups were assessed by unpaired *t* test or 1-way or 2-way analysis of variance as specified in the legends. All statistical analyses were performed in the GraphPad Prism 7.0 software. A *P* value of .05 or less was considered statistically significant.

Results

BAs Stimulate Intestinal Organoid Growth Through TGR5

Chronic high-fat diet (HFD) feeding is not only associated with an expansion of the $Lgr5^+$ ICS compartment,[4] but also with elevated BA levels.[25] To investigate whether a causal relationship may exist between BAs and ICS function, we fed mice with either chow diet or HFD for 21 weeks (Supplementary Figure 1*A*). In line with the previous literature, HFD induced the expression of the ISC marker *Lgr5* and this induction correlated with a marked accumulation of fecal BAs (Figure 1*A* and *B*). In $Tgr5^{-/-}$ mice, however, HFD failed to induce *Lgr5*, despite a persistent increase in the fecal BA size (Figure 1*A* and *B*), suggesting a putative role of BA-responsive TGR5 axis in controlling intestinal stemness.

To better understand the exact role of BAs in controlling intestinal cell renewal, we assessed the ability of isolated epithelial crypts to form clonogenic organoids as an ex vivo assay of ISC function.[26] In the gut, primary BAs are metabolized by the resident microbiota into secondary BAs. To mimic the in vivo situation, freshly isolated mouse intestinal crypts were embedded in Matrigel to allow organoid

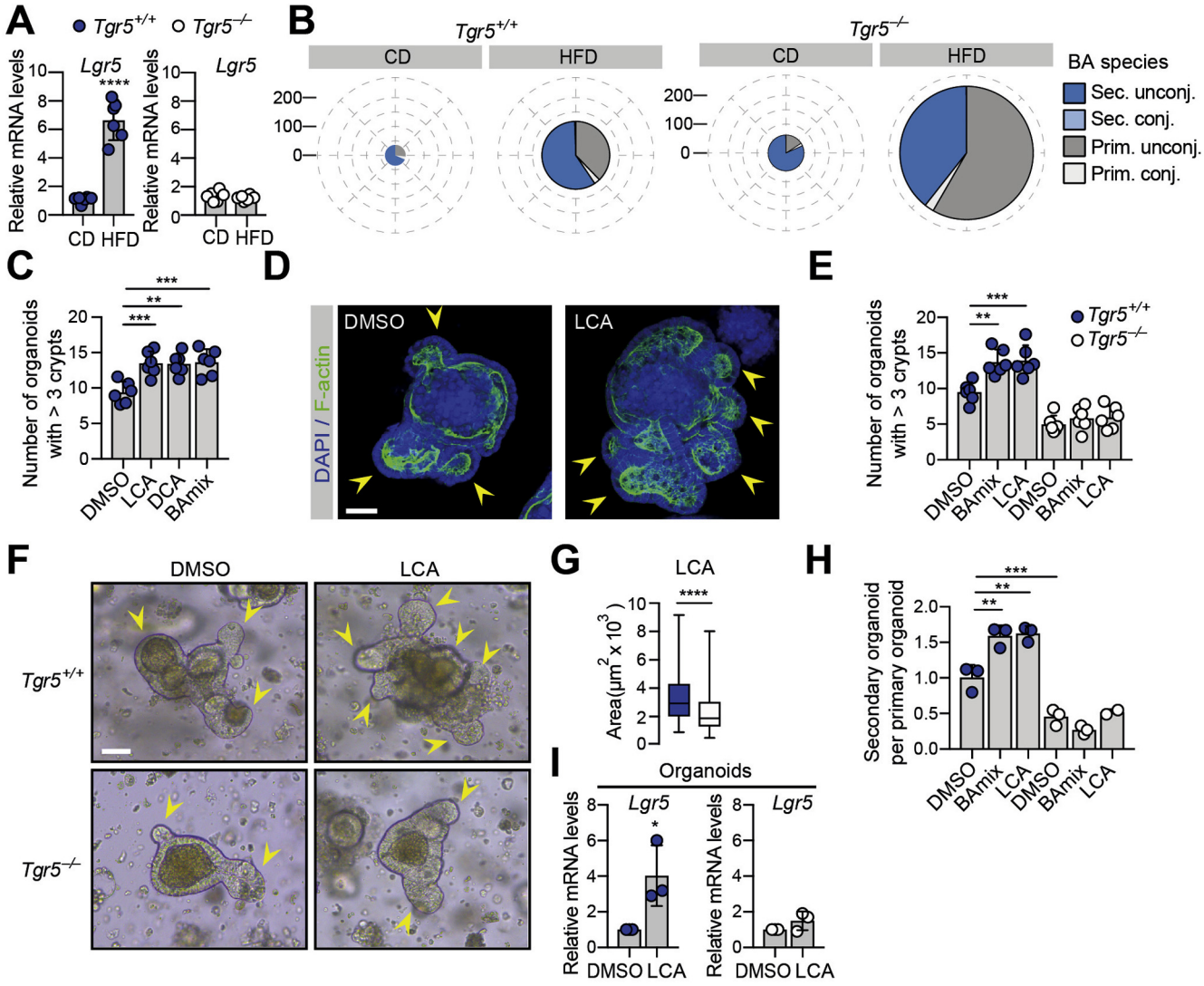

Figure 1. BAs promote organoid growth via TGR5. (*A*) Quantitative reverse-transcriptase polymerase chain reaction (qRT-PCR) analysis for stem cell marker *Lgr5* in duodenal samples from *Tgr5*$^{+/+}$ and *Tgr5*$^{-/-}$ mice fed either chow diet or HFD for 21 weeks. (*B*) Pie charts representing the BA abundance (pie size) and composition (different colors specified in the legend) in feces collected over a 24-hour period in the experimental cohorts described in (*A*). (*C*) Intestinal crypts were isolated from C57BL/6J mice, embedded in Matrigel, and exposed to LCA (10 μM), DCA (10 μM), or BAmix (10 μg/mL) for 6 days. The organoid buddings were quantified and statistical analysis was performed (n = 6 biological replicates). (*D*) Representative images relative to (*C*). *Yellow arrowheads* indicate crypt domains. Scale bar (50 μm). (*E*) Intestinal crypts were isolated from *Tgr5*$^{+/+}$ or *Tgr5*$^{-/-}$ mice, embedded in Matrigel, and exposed to BAmix (10 μg/mL) or LCA (10 μM) for 6 days. The organoid buddings were quantified for statistical analysis (n = 6 mice per genotype). (*F*) Representative images of organoids exposed to dimethyl sulfoxide (DMSO) or LCA for 6 days. *Yellow arrowheads* indicate crypt domains. Scale bar (50 μm). (*G*) Quantification of the size of organoids derived from indicated genotypes and exposed to LCA (10 μM) for 6 days (n = 102 organoids per genotype). (*H*) Organoid forming capacity of sub-cultured mouse organoids (n = 3 mice per genotype). (*I*) qRT-PCR analysis for stem cell marker *Lgr5* in organoids from indicated genotypes and exposed to LCA (10 μM) for 6 days (n = 3 mice per genotype). Graphs represent mean ± SD. $^{**}P < .01$, $^{***}P < .001$, $^{****}P < .0001$. *P* values were calculated using 1-way analysis of variance (*C*, *E*, *H*) or 2-tailed Student *t* test (*A*, *G*, *I*).

generation, and exposed to physiological doses of the secondary BAs, LCA or DCA, or a crude bile extract (BAmix) containing both primary and secondary BAs.[27] We observed that exposure to BAs for 6 days triggered the growth of de novo crypts, as reflected by the increased number of buds per organoid, suggesting improved stem cell function[4,5] (Figure 1*C* and *D* and Supplementary Figure 1*B*). In line with the documented toxicity of secondary BA overload,[28] exposure to high doses of LCA, instead, was associated with a significant reduction of organoid number (Supplementary Figure 1*C*).

We next assessed the expression of TGR5 in intestinal organoids and found that it was maintained in vitro (Supplementary Figure 1*D*). To study the role of TGR5 on BA-driven organoid growth, organoids from crypts isolated from whole-body *Tgr5* knockout mice (*Tgr5*$^{-/-}$) were

exposed to either LCA or BAmix. Of note, in the absence of TGR5, BAs failed to increase the number of organoid buds, indicating that BAs stimulate organoid growth via TGR5 activation (Figure 1*E* and *F*). In further support of this notion, the size of *Tgr5*$^{-/-}$ organoids was significantly smaller compared with their wild-type counterpart when LCA was added to the medium (Figure 1*G*). To test the impact of TGR5 on TA cell proliferation, we performed EdU labeling assay. We found that BAmix-exposed organoids derived from *Tgr5*$^{-/-}$ mice showed a marked reduction in EdU-positive cells when compared with wild-type organoids (Supplementary Figure 1*E*), indicating that TGR5 stimulation by BAs promotes progenitor cell proliferation. We then evaluated the impact of BAs on ISC self-renewal, a process necessary for intestinal regeneration. When subcloned, BA-exposed primary organoids generated more secondary organoids as compared with control organoids, and this effect was completely abolished in organoids derived from *Tgr5*$^{-/-}$ mice (Figure 1*H*). In line with these results, LCA exposure increased the expression of the ISC marker *Lgr5*, but not that of quiescent "+4" stem cells[29] (Supplementary Figure 1*F*), whereas this effect was absent in *Tgr5*$^{-/-}$ organoids (Figure 1*I*). To rule out the possibility that BAs affect organoid growth via the muscarinic M3 receptor, which was previously shown to be activated by LCA in cancer cells,[30] we inhibited its activation by exposure to the specific antagonist 4-DAMP[31] and found that this condition was unable to prevent organoid growth on LCA stimulation (Supplementary Figure 1*G*). Altogether, these data unveil a key role of the BA-TGR5 axis in coordinating intestinal organoid proliferation and ISC function.

TGR5 Controls ISC Function Ex Vivo and In Vivo

In situ hybridization revealed that jejunal *Tgr5* expression is scattered along the intestinal villus-crypt axis (Supplementary Figure 2*A*). However, *Tgr5* also could be detected in the ISC pool, as several *Lgr5*$^{+}$ cells scored positive for *Tgr5* (Figure 2*A* and Supplementary Figure 2*B*). To corroborate these data, we took advantage of the Lgr5-EGFP-IRES-CreERT2 knockin mouse model (*Lgr5-Tg*), which expresses both GFP and the tamoxifen-inducible Cre recombinase (CreERT2) in the ISCs, hence allowing their purification by FACS,[21] here referred to as GFP^{hi} subpopulation. We measured *Tgr5* messenger RNA levels in purified GFP^{hi} cells and found that *Tgr5* was highly expressed in the ISC population, as compared with the bulk of differentiated cells (defined as the GFP^{neg} cells) (Supplementary Figure 2*C*), raising the possibility that ISCs could respond to BA stimulation. To assess the effect of BAs specifically on ISCs, intestinal organoids were generated from *Lgr5-Tg* reporter mice and exposed to LCA. As shown in Figure 2*B*, LCA exposure induced a significant expansion of the GFP^{+} cell population. Next, ISC cells were isolated from the mouse intestinal epithelium by FACS sorting and embedded in Matrigel for ex vivo expansion in an established growing medium,[21] in the absence or presence of BAmix or LCA. Of note, exposure to BAs improved renewal and crypt formation as indicated by quantification of the number of buds (Figure 2*C*).

To characterize the role of BA-TGR5 signaling in ISCs, we next generated mice with a conditional *Tgr5* disruption in the ISC pool. To this aim, we crossed the *Lgr5-Tg* mice with mice carrying floxed *Tgr5* alleles (*Tgr5*$^{fl/fl}$)[12] (Figure 2*D*), and generated ISC-specific *Tgr5* knockout mice (*Tgr5*$^{ISC-/-}$) by tamoxifen administration. As expected, *Tgr5* expression was significantly blunted in ISCs from *Tgr5*$^{ISC-/-}$ mice but not from vehicle-exposed *Lgr5-Tg/Tgr5*$^{fl/fl}$ (*Tgr5*$^{ISC+/+}$) mice, and *Tgr5* deletion was maintained for at least 3 weeks (Supplementary Figure 2*D*–*F*). Of interest, *Tgr5* deletion in ISCs triggered a marked reduction in stem cell number (Figure 2*E* and Supplementary Figure 2*G* and *H*), and this effect was independent of tamoxifen administration (Supplementary Figure 2*I*). In line with these findings, immunostaining revealed a significantly lower number of ISCs in the crypts of *Tgr5*$^{ISC-/-}$ mice in vivo (Figure 2*F*), further supporting a role for TGR5 in ISC homeostasis. We then tested the impact of *Tgr5* deletion in vivo on ISC function ex vivo. ISCs were isolated from vehicle (*Tgr5*$^{ISC+/+}$) and tamoxifen-exposed (*Tgr5*$^{ISC-/-}$) mice and plated in Matrigel-based culture. Remarkably, stem cells isolated from *Tgr5*$^{ISC-/-}$ mice were much less efficient in generating organoids as compared with control mice (Figure 2*G* and Supplementary Figure 2*J*). Moreover, the growth of organoids generated from ISCs lacking *Tgr5* was no longer responsive to LCA exposure (Figure 2*H* and Supplementary Figure 2*K*). Taken together, these results demonstrate that an active BA-TGR5 signaling is required to maintain ISC homeostasis and function.

TGR5 Activation in ISCs Controls Intestinal Proliferation and Cell Specification

To test whether activation of TGR5 by the endogenous BA pool has any physiological impact on the proliferation of intestinal crypts in vivo, we quantified the number of proliferating cells in the small intestine of tamoxifen-exposed *Tgr5*$^{fl/fl}$ and *Tgr5*$^{ISC-/-}$ mice by means of EdU assay. Interestingly, loss of *Tgr5* in ISCs resulted in a marked reduction of the number of proliferating cells in both stem cell and progenitor compartments (Figure 3*A* and *B* and Supplementary Figure 3*B*). Moreover, although crypts from *Tgr5*$^{ISC-/-}$ mice appeared morphologically healthy, they were significantly shorter compared with control mice (Supplementary Figure 3*A*).

We next tested whether the BA-TGR5 axis impacts on the generation of terminally differentiated cells, a process initiated by ISCs. Disruption of *Tgr5* in ISCs did not change the number of enterocytes and Paneth cells, as assayed by Fatty acid binding protein 1 (L-FABP) and Lysozyme (LYZ) staining, respectively (Figure 3*C* and Supplementary Figure 3*C* and *D*). However, the number of Periodic acid–Schiff–positive cells and Chromogranin A (ChgA)-positive cells was significantly attenuated in *Tgr5*$^{ISC-/-}$ mice, suggesting that ISCs require TGR5 for normal differentiation into Goblet cells and

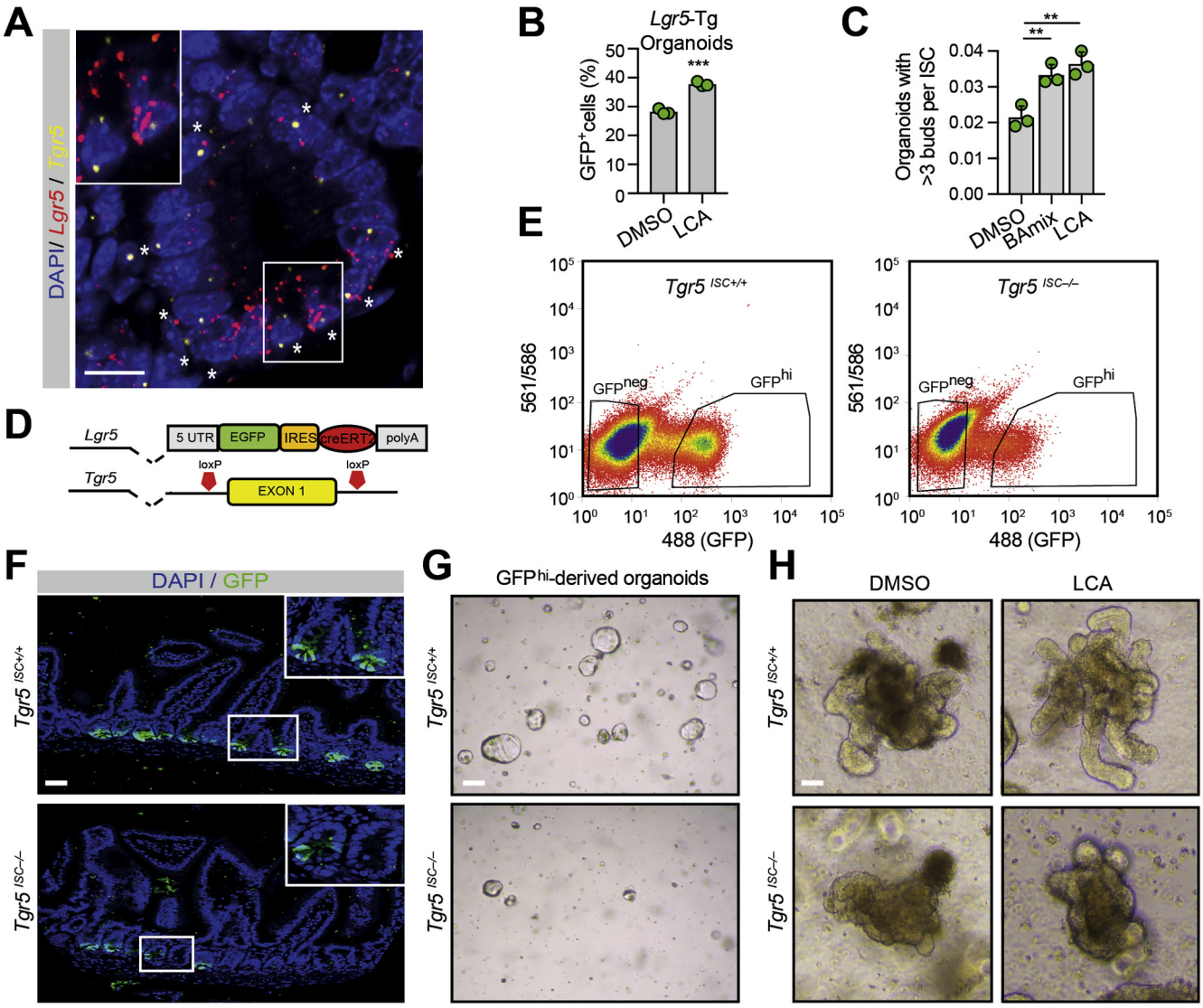

Figure 2. TGR5 is expressed in Lgr5^{+} cells and controls ISC homeostasis. (*A*) *Lgr5* (*red dots*) and *Tgr5* (*yellow dots*) in situ hybridization was performed in duodenum sections from C57BL/6J mice. Asterisks indicate *Lgr5*/*Tgr5* double-positive cells. Scale bar (10 μm). (*B*) Percentage of GFP^{+} cells in intestinal organoids measured by flow cytometry after exposure to dimethyl sulfoxide (DMSO) or LCA (10 μM) for 3 days. (*C*) ISCs isolated from Lgr5-Tg mice were cultured for organoid formation and exposed to BAmix (10 μg/mL) or LCA (10 μM) for 9 days. The organoid buddings were quantified for statistical analysis (n = 3 mice). (*D*) Schematic representation of the generation of mice expressing EGFP and CreERT2 from a single bicistronic sequence that was inserted into the first exon of *Lgr5*, crossed with mice carrying lox sequences flanking exon 1 of the *Tgr5* gene. (*E*) GFP^{hi} and GFP^{neg} cells in the entire small intestine monitored by flow cytometry after 7 days on last tamoxifen administration. (*F*) Lgr5-GFP^{+} cells were imaged by confocal cross-sectioning of jejunal intestinal samples from indicated genotypes. Scale bar (50 μm). (*G*) Organoid-initiating capacity of GFP^{hi} cells isolated by flow cytometry from indicated genotypes after 2 days in culture. Representative images are shown (n = 5 mice per genotype). Scale bar (50 μm). (*H*) Representative images of isolated GFP^{hi} cells exposed to DMSO or LCA for 9 days. Scale bar (50 μm). Graphs represent mean ± SD. $^{**}P < .01$, $^{***}P < .001$. *P* values were calculated using 1-way analysis of variance (*C*) or 2-tailed Student *t* test (*B*).

enteroendocrine cells (Figure 3*C* and Supplementary Figure 3*E* and *F*). Moreover, in line with recently published findings,[32] quantification of Glucagon-positive (Gluc^{+}) cells[33] in jejunal samples demonstrated an equally impaired efficiency of ISCs to differentiate into L-cells in the absence of *Tgr5* (Figure 3*D*). Conversely, LCA exposure in organoids induced the expression of Goblet and enteroendocrine cell markers (Supplementary Figure 4*A*). These in vivo and ex vivo findings demonstrate that BA-TGR5 signaling is not only required for ISC self-renewal and progenitor proliferation, but also for their proper specification into different epithelial lineages.

Diet-derived nutrients of lipid-like origin have been shown to enhance stemness in the gut.[4,34] Because BAs are physiological lipid emulsifiers and acutely rise in the intestinal lumen after food intake, we wondered whether this postprandial physiological response might be sufficient to

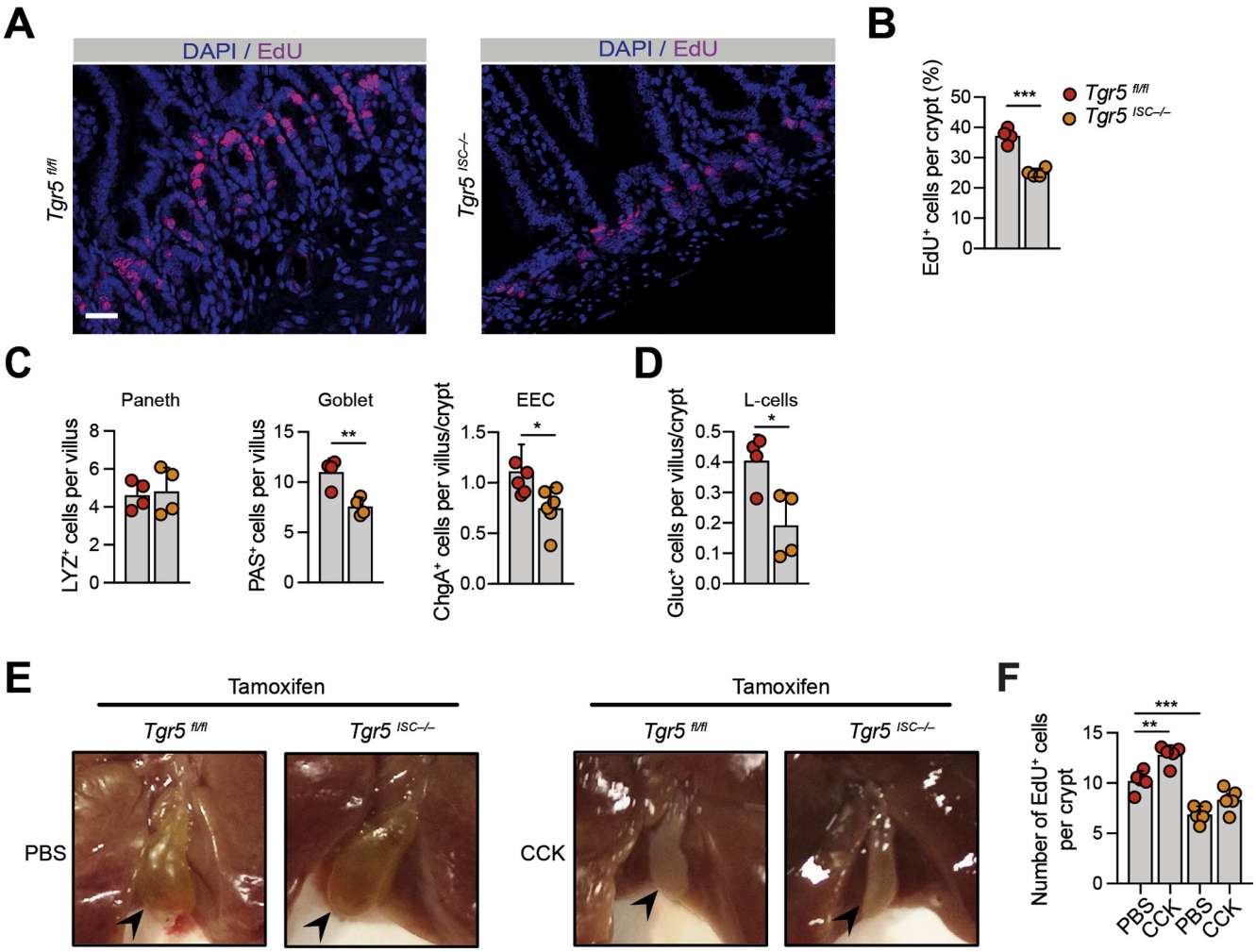

Figure 3. TGR5 controls homeostatic intestinal cell renewal and specification. (*A* and *B*) Representative images (*A*) and quantification (*B*) of EdU$^+$ proliferating cells in jejunal samples from mice of indicated genotypes, after a 2-hour pulse. Scale bar (50 μm). (*C*) Quantification of Paneth cells (Lysozyme-positive cells, n = 4 mice per genotype), Goblet cells (Periodic acid-Shiff–positive cells, n = 4 mice per genotype), enteroendocrine cells (Chromogranin A–positive cells, n = 6 mice per genotype) in jejunal intestinal samples from indicated genotypes. (*D*) Quantification of L-cells (Glucagon-positive cells, n = 4 mice per genotype) in jejunal intestinal samples from indicated genotypes. **(***E*) Representative images showing gallbladder of overnight fasted mice, 30 min after intraperitoneal injection of PBS (*left*) or CCK (200 μg/kg; right). (*F*) Quantification of EdU$^+$ proliferating cells in duodenal samples from mice of indicated genotypes, 30 minutes after vehicle (PBS) or cholecystokinin (CCK) (200 μg/kg) intraperitoneal injection. Graphs represent mean ± SD. $^*P < .05$, $^{**}P < .01$, $^{***}P < .001$. *P* values were calculated using 1-way analysis of variance (*F*) or 2-tailed Student *t* test (*B*, *C*, *D*).

trigger ISC-mediated intestinal proliferation. To avoid the confounding effects of diet-derived nutrients on ISC function, we decided to bypass the requirement of food intake for BA secretion. To this aim, we experimentally mimicked the effect of food ingestion on gallbladder contraction by giving to fasted mice CCK, a hormone secreted in response to a meal and known to stimulate gallbladder contraction and BA release into the intestinal lumen. As expected, injection of CCK efficiently triggered the contraction of the gallbladder of both fasted control and *Tgr5*$^{ISC-/-}$ mice (Figure 3*E*), causing a massive and complete release of BAs into the duodenum. Three hours after CCK injection, a moderate but significant increase in the number of proliferating cells was evident in controls, but not in *Tgr5*$^{ISC-/-}$ mice (Figure 3*F*), and *Tgr5* was expressed in most proliferating cells in CCK-exposed mice (Supplementary Figure 3*G*). These results demonstrate that intestinal epithelial turnover is influenced by the activity of endogenous BAs and that the acute increase of their intestinal concentration by physiological stimuli boosts the intestinal proliferation rate.

TGR5 Improves the Regenerative Capacity of Damaged Epithelium in Experimentally Induced Colitis

To assess the importance of BAs on intestinal damage and ISC-mediated tissue regeneration, we induced experimental colitis in our mouse model by means of DSS (Figure 4*A*). DSS significantly worsened colitis in *Tgr5*$^{ISC-/-}$

mice compared with tamoxifen-exposed *Tgr5*$^{fl/fl}$ mice, as evidenced by an accelerated and more pronounced weight loss, as well as a marked reduction in colon length, 2 clinical indices of disease activity (Figure 4*B*–*E* and Supplementary Figure 4*B*). Consistent with these data, the histopathological score was higher in *Tgr5*$^{ISC-/-}$ mice (Figure 4*F* and *G*), showing larger ulcerations (Supplementary Figure 4*C* and *D*) and a more extensive crypt loss (Figure 4*F*). Moreover, spleen weight of *Tgr5*$^{ISC-/-}$ mice was significantly increased (Figure 4*H*), suggesting enhanced inflammation. Finally, *Tgr5*$^{ISC-/-}$ mice were more susceptible than *Tgr5*$^{fl/fl}$ mice to loss of intestinal barrier function, as assayed by the extent of disseminated intestinal bacteria in the spleen (Figure 4*I*). Interestingly, when mice were subjected to the same DSS protocol and then transferred to normal drinking water for 3 days to promote regeneration (Figure 4*J*), the colonic crypts showed marked proliferative defects in *Tgr5*$^{ISC-/-}$ mice, suggesting that activation of TGR5 is necessary to support intestinal regeneration and ensure complete epithelial healing after acute insults (Figure 4*K* and *L*). Altogether, these results demonstrate that loss of TGR5 function in ISCs leads to an accelerated onset and progression of DSS-induced colitis, together with an impaired regenerative capacity.

TGR5 Stimulation Activates a SRC/YAP-dependent Regenerative Program

To gain insight into the mechanisms by which stimulation of the BA-TGR5 axis promotes intestinal regeneration, we performed RNA sequencing on isolated ISCs exposed to the TGR5 selective agonist, INT-777 (Supplementary Figure 5*A*).[12] Analysis of the promoters of genes that were upregulated by INT-777 showed enrichment of TEADs binding motifs (Supplementary Figure 5*B*–*D*). TEADs are a family of transcription factors known to control gene expression in complex with the transcription cofactor YAP.[35] YAP is the nuclear transducer of the Hippo pathway and plays a central role in gut physiology, more particularly in promoting epithelial regeneration.[36] Although aberrant BA levels have been proposed to promote YAP activation leading to cancer development in the liver[37] and metastatic dissemination in the lymph nodes,[38] the existence of a functional crosstalk between TGR5 and YAP in controlling gut regeneration has never been investigated. To test whether TGR5 activation promotes the nuclear localization and thus activity of YAP,[39] we isolated GFP^{hi} ISCs by FACS and embedded them in Matrigel to allow organoid formation. In line with recently reported data, Lgr5^{+} cells were reprogrammed by transient YAP activation, a phenomenon required to ensure a swift reconstitution of the pool of Lgr5^{+} cells and coordination of the mucosal regenerative program (Figure 5*A*). Of note, TGR5 activation by INT-777 was able to protract YAP nuclear localization in organoids, and amplify the magnitude of its activation (Figure 5*A* and Supplementary Figure 6*A*). To corroborate these findings, we isolated Lgr5^{+} cells and assessed YAP transcriptional activation after INT-777 exposure for 3 days. Remarkably, exposure to INT-777 significantly induced a series of canonical YAP target genes[40] as well as several markers of fetal intestinal progenitors (Figure 5*B*), known to be associated with YAP-driven intestinal regeneration.[41] Moreover, blocking the physical interaction between YAP and TEAD by means of Verteporfin[42] exposure from day 3 to day 5 abolished the effect of TGR5 activation on organoid growth (Figure 5*C* and Supplementary Figure 6*B* and *C*). These results demonstrate that TGR5 stimulation during organoid growth potentiates the YAP regenerative program, that is functionally required for BA-mediated organoid growth.

On tissue damage, the tyrosine kinase SRC serves as a signaling hub that integrates mechanical and inflammatory stimuli to initiate, through direct phosphorylation, the YAP-dependent regenerative program.[41] In pathological settings, such as colorectal cancer and viral infection, secondary BAs have been shown to promote SRC kinase activity.[43,44] Therefore, we postulated that in the intestinal epithelium SRC might mediate the effects of an activated TGR5 signaling pathway on YAP. To examine this possibility, we exposed ISCs with INT-777 for 3 days and then monitored SRC and YAP activity. In line with our hypothesis, INT-777 induced phosphorylation of the SRC activation loop (pY-418),[45] and robustly phosphorylated YAP on its SRC-specific target site (pY-357) (Figure 5*D*).[46] Moreover, inhibition of SRC by Dasatinib[47] exposure phenocopied the effect of Verteporfin in preventing BA-induced organoid growth (Figure 5*C* and Supplementary Figure 6*B* and *C*). These results demonstrate that TGR5 stimulation during organoid growth potentiates the SRC/YAP regenerative program that is functionally required for BA-mediated organoid growth.

TGR5 Activation Promotes Lgr5^{+} Stem Cell Pool Reconstitution On Tissue Damage

Although *Lgr5*$^{+}$ stem cells are lost following injury,[39,48] they are readily reconstituted de novo on damage removal to orchestrate intestinal regeneration.[49] In this context, recent evidence showed that transient YAP activation is critically required for the reconstitution of the Lgr5 cell pool allowing subsequent epithelium regeneration.[39,49,50] To test the role of TGR5 in this process, we isolated ISCs and monitored *Lgr5*$^{+}$ cells during organoid growth. As expected, *Lgr5*-expressing cells were completely lost after 24 hours in culture (Figure 5*E*). However, after 5 days in culture, *Lgr5*$^{+}$ cells re-appeared and after 7 days they generated fully mature organoids with *Lgr5*$^{+}$ crypts (Figure 5*E*). Of note, in this experimental setting, INT-777 exposure promoted de novo *Lgr5*$^{+}$ cell regeneration as suggested by the appearance of mature organoids containing more *Lgr5*$^{+}$ crypts (Figure 5*E* and *F*). Importantly, transient inhibition of SRC and YAP from day 3 to day 5 (the timeframe in which INT-777 maintains YAP active in the organoids), was able to efficiently prevent this effect (Figure 5*F* and Supplementary Figure 6*D*). To confirm the role of TGR5 in promoting SRC/YAP activation and Lgr5^{+} pool reconstitution in vivo, we monitored SRC and YAP in recovering intestinal epithelium 3 days after DSS-induced injury. We observed that Tgr5 deletion in ISCs reduced the activation of SRC and YAP at the plasma membrane and in the nucleus of GFP^{+} regenerating

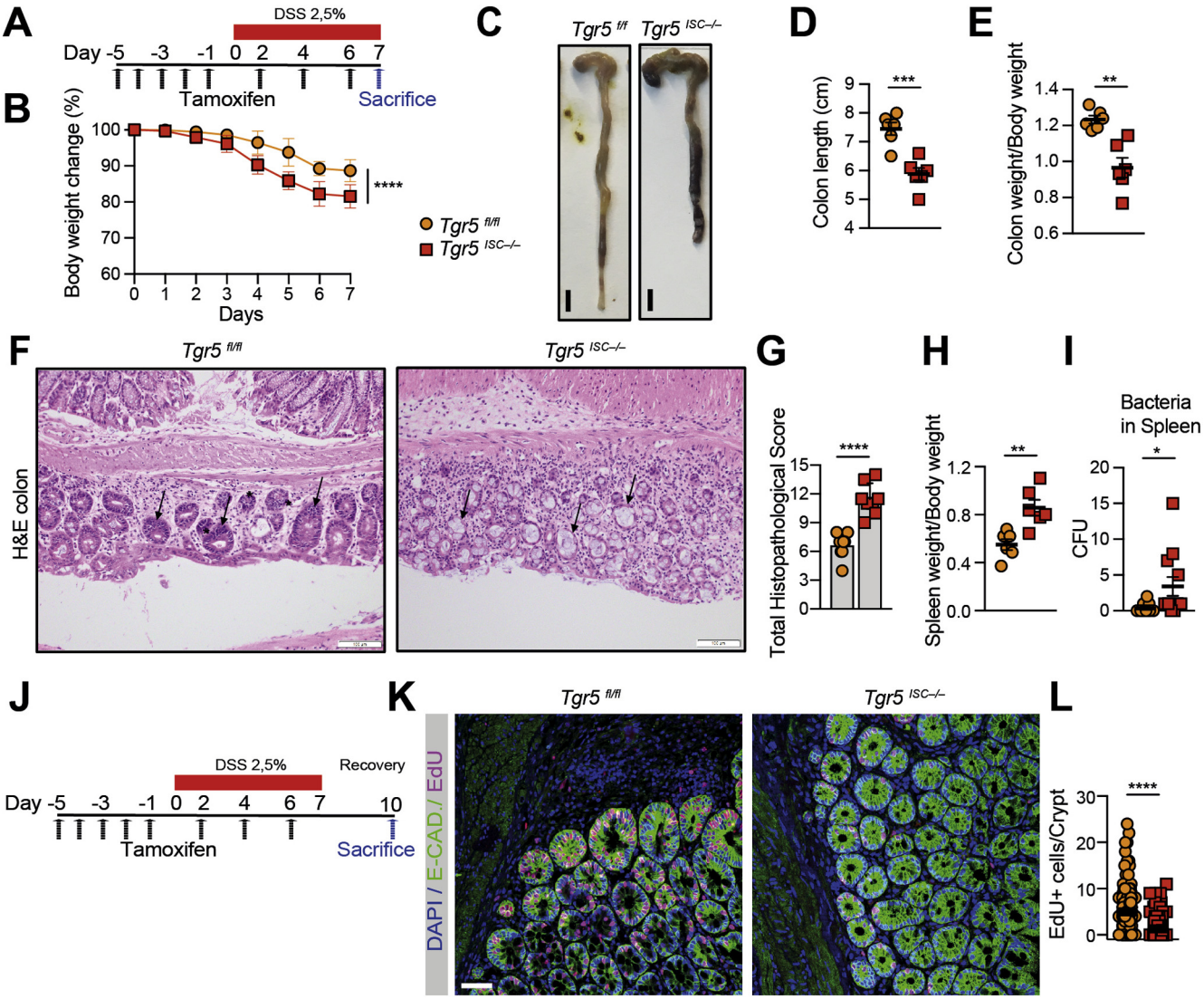

Figure 4. TGR5 controls experimental colitis susceptibility and is required for intestinal epithelium regeneration. (*A*) Workflow of acute DSS-induced colitis experiment. Mice were daily injected with tamoxifen for 5 consecutive days followed by DSS (2.5%) exposure for 7 days. Tamoxifen was also administered every 2 days during DSS exposure. (*B*) Percentage of body weight loss during DSS exposure. (*C*) Representative image of colons from the indicated genotypes at the time mice were killed (day 7 after DSS initiation). (*D* and *E*) Colon length (*D*) and weight (*E*) from mice of the indicated genotypes at the time mice were killed (day 7 after DSS initiation). (*F*) Representative histological images of colon from DSS-exposed mice of the indicated genotypes. Multiple layers of high columnar cryptal epithelial cells (hyperplasia, *arrow*) and frequent mitotic crypts (*asterisk*) are highlighted in control mice. Scale bar (100 μm). (*G*) Total histopathological score (sum of the following parameters: severity of inflammation, ulceration, crypt damage) of the indicated genotypes at the time mice were killed (day 7 after DSS initiation). (*H*) Spleen weight normalized to body weight, at the time mice were killed (day 7 after DSS initiation). (*I*) Bacterial colony-forming units (CFU) in the spleen. (*J*) Workflow of acute DSS-induced colitis experiment. Mice were daily injected with tamoxifen for 5 consecutive days followed by DSS (2.5%) exposure in the drinking water for 7 days and then by water for 3 additional days (recovery). (*K* and *L*) Representative images (*K*) and quantification (*L*) of EdU$^+$ cells in colon from DSS-exposed mice of the indicated genotypes (day 3 after DSS withdrawal). Scale bar (50 μm). Graphs represent mean ± SD. $^*P < .05$, $^{**}P < .01$, $^{***}P < .001$, $^{****}P < .0001$. *P* values were calculated using 2-way analysis of variance (*B*) or 2-tailed Student *t* test (*D*, *E*, *G*, *H*, *I*, *L*).

crypts, respectively (Figure 5*G*). In line with our in vitro results, DSS induced a prominent reduction of GFP$^+$ cells, which efficiently regenerated after DSS removal in the jejunum of control mice (Figure 5*G* and Supplementary Figure 6*E*). Of note, this event was markedly impaired in *Tgr5*$^{ISC-/-}$ mice (Figure 5G and Supplementary Figure 6*E*). Altogether, these results demonstrate that, following intestinal damage, TGR5 activation supports the reconstitution of the *Lgr5*$^+$ ISC pool required for proper healing of the gut epithelium.

Discussion

In conclusion, our findings establish a novel role of BAs as regulatory components of the ISC niche and shed light on the complex question of how the nutritional state of an

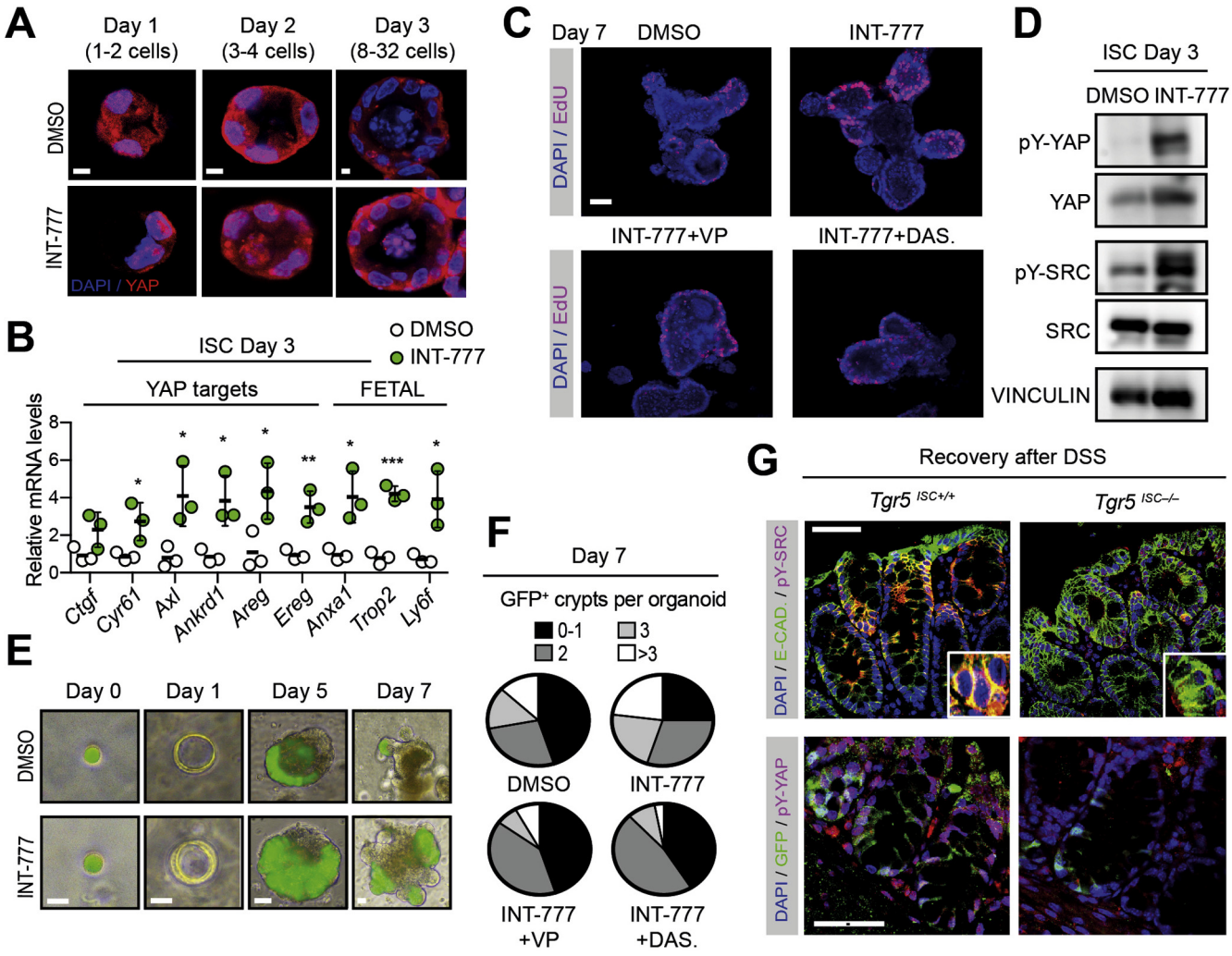

Figure 5. TGR5 stimulation activates an SRC/YAP-dependent regenerative program. (*A*) YAP localization in organoids generated from single GFP^{hi} cells and exposed to dimethyl sulfoxide (DMSO) or INT-777 (30 μM) for indicated time. Scale bar (10 μm). (*B*) Quantitative reverse-transcriptase polymerase chain reaction (qRT-PCR) of YAP target genes and fetal intestinal markers in organoids generated from single GFP^{hi} cells exposed to DMSO or INT-777 (30 μM) for 3 days (n = 3 biological replicates). (*C*) Crypts were embedded in Matrigel and exposed to DMSO or INT-777 (30 μM) until day 7. From day 3, Verteporfin (VP, 1 μM) and Dasatinib (DAS, 50 nM) were added in the culture medium. Representative images of EdU incorporation in organoids are shown. Scale bar (50 μm). (*D*) Western blot was performed from organoids generated from single GFP^{hi} cells exposed to DMSO or INT-777 (30 μM) for 3 days (experiment performed 3 times). (*E*) Brightfield/epifluorescent image overlay of organoids generated from single isolated GFP^{hi} cells at indicated time points. Scale bar (10 μm). (*F*) Quantification of the number of GFP^{+} crypt per organoid 7 days after INT-777 (30 μM) exposure. Verteporfin (VP, 1 μM) and Dasatinib (DAS, 50 nM) were added from day 3 to day 5. **(***G*) Detection of pY-SRC, E-cadherin (E-CAD, for plasma membrane staining), pY-YAP, and GFP (for detecting Lgr5^{+} cells) during the repair phase by confocal microscopy in colons from indicated genotypes. Scale bar (50 μm). Graphs represent mean ± SD. *$P < .05$, **$P < .01$, ***$P < .001$. *P* values were calculated using 2-tailed Student *t* test.

organism may affect stem cell functions. In particular, we showed that BAs foster epithelial regeneration via activation of the plasma membrane receptor TGR5 in the ISC compartment and demonstrated that endogenous BA release in the intestinal lumen is sufficient to coordinate ICS renewal and proliferation. These findings suggest that the physiological cycles of food intake followed by discharge of BAs in the intestinal lumen represent an intrinsic stimulus that dictates ISC proliferation rhythms to sustain daily regeneration. Our study also revealed that the BA-TGR5 axis is required to reprogram the intestinal epithelium into a proliferative repairing tissue through ISC recovery and gut regeneration. Mechanistically, we identified activation of YAP as a key signaling event downstream of TGR5 stimulation during intestinal regeneration and that activation of the SRC kinase is required downstream of TGR5 to unleash the YAP-dependent regenerative program.

In full accordance with our data, a recent article reported that reduction of endogenous levels of secondary BAs is observed in patients with ulcerative colitis and that reconstitution of physiological levels of BAs by rectal administration of LCA is able to alleviate murine colitis through a mechanism involving TGR5-dependent

anti-inflammatory effects.[51] These findings, together with our results, imply that BAs, through TGR5, likely promote intestinal healing via a dual mechanism encompassing an anti-inflammatory activity on gut resident immune cells and a pro-regenerative program in epithelial cells.

The colonic regenerative response involves a finely tuned, self-limiting series of cellular and molecular events orchestrated by the transient activation of epithelial stem cells. However, chronic and aberrant initiation of wound healing processes has been shown to promote the expansion of cancer cells with stem-like properties that ultimately promote cancer progression.[52] In accordance with this notion, epidemiological studies have shown that higher levels of unconjugated secondary BAs, such as DCA and LCA, in patients who consumed high-fat/low-fiber diets represent risk factors for colorectal cancer development.[53,54] Data from in vitro and in vivo studies have unveiled a paramount role of BAs in promoting the expansion of cancer stem cells (CSCs) in the intestinal epithelium. This has been highlighted by the evidence that BAs boost CSC phenotypes and increase the number and proliferation of transformed $Lgr5^{+}$ CSCs in a HFD-fed mouse model of colorectal cancer.[53,54]

From a therapeutic angle, an important implication of our work is that although chronic activation of the BA signaling could be dangerous, acute or short-term targeting of intestinal TGR5 with selective and potent agonists could constitute a novel strategy to enhance the regenerative capacity of the intestinal epithelium in patients with defective or delayed intestinal repair capacity, such as seen in patients with inflammatory bowel disease after a flare-up of the disease, or in patients with cancer subjected to chemo- or radiotherapy. Future studies should be directed at testing this intriguing hypothesis in clinical settings.

Supplementary Material

Note: To access the supplementary material accompanying this article, visit the online version of *Gastroenterology* at www.gastrojournal.org, and at https://doi.org/10.1053/j.gastro.2020.05.067.

References

1. Williams JM, Duckworth CA, Burkitt MD, et al. Epithelial cell shedding and barrier function: a matter of life and death at the small intestinal villus tip. Vet Pathol 2015;52:445–455.
2. Peterson LW, Artis D. Intestinal epithelial cells: regulators of barrier function and immune homeostasis. Nat Rev Immunol 2014;14:141–153.
3. Barker N. Adult intestinal stem cells: critical drivers of epithelial homeostasis and regeneration. Nat Rev Mol Cell Biol 2014;15:19–33.
4. Beyaz S, Mana MD, Roper J, et al. High-fat diet enhances stemness and tumorigenicity of intestinal progenitors. Nature 2016;531:53–58.
5. **Yilmaz ÖH, Katajisto P**, Lamming DW, et al. mTORC1 in the Paneth cell niche couples intestinal stem-cell function to calorie intake. Nature 2012;486:490–495.
6. Cheng C-W, Biton M, Haber AL, et al. Ketone Body Signaling Mediates Intestinal Stem Cell Homeostasis and Adaptation to Diet. Cell 2019;178:1115–1131.e15.
7. **McLeod CJ, Wang L**, Wong C, et al. Stem cell dynamics in response to nutrient availability. Curr Biol 2010;20:2100–2105.
8. Richmond CA, Shah MS, Deary LT, et al. Dormant intestinal stem cells are regulated by PTEN and nutritional status. Cell Rep 2015;13:2403–2411.
9. **Mihaylova MM, Cheng C-W**, Cao AQ, et al. Fasting activates fatty acid oxidation to enhance intestinal stem cell function during homeostasis and aging. Cell Stem Cell 2018;22:769–778.e4.
10. Wahlström A, Sayin SI, Marschall H-U, et al. Intestinal crosstalk between bile acids and microbiota and its impact on host metabolism. Cell Metab 2016;24:41–50.
11. Thomas C, Pellicciari R, Pruzanski M, et al. Targeting bile-acid signalling for metabolic diseases. Nat Rev Drug Discov 2008;7:678–693.
12. Thomas C, Gioiello A, Noriega L, et al. TGR5-mediated bile acid sensing controls glucose homeostasis. Cell Metab 2009;10:167–177.
13. **Pols TWH, Nomura M**, Harach T, et al. TGR5 Activation inhibits atherosclerosis by reducing macrophage inflammation and lipid loading. Cell Metab 2011;14:747–757.
14. **Watanabe M, Houten SM**, Mataki C, et al. Bile acids induce energy expenditure by promoting intracellular thyroid hormone activation. Nature 2006;439:484–489.
15. Perino A, Pols TWH, Nomura M, et al. TGR5 reduces macrophage migration through mTOR-induced C/EBPβ differential translation. J Clin Invest 2014;124:5424–5436.
16. Perino A, Schoonjans K. TGR5 and immunometabolism: insights from physiology and pharmacology. Trends Pharmacol Sci 2015;36:847–857.
17. Pols TWH, Noriega LG, Nomura M, et al. The bile acid membrane receptor TGR5 as an emerging target in metabolism and inflammation. J Hepatol 2011;54:1263–1272.
18. Alemi F, Poole DP, Chiu J, et al. The receptor TGR5 mediates the prokinetic actions of intestinal bile acids and is required for normal defecation in mice. Gastroenterology 2013;144:145–154.
19. Cipriani S, Mencarelli A, Chini MG, et al. The bile acid receptor GPBAR-1 (TGR5) modulates integrity of intestinal barrier and immune response to experimental colitis. PLoS One 2011;6:e25637.
20. Zietek T, Rath E, Haller D, et al. Intestinal organoids for assessing nutrient transport, sensing and incretin secretion. Sci Rep 2015;5:16831.
21. Barker N, Es JH van, Kuipers J, et al. Identification of stem cells in small intestine and colon by marker gene Lgr5. Nature 2007;449:1003–1007.
22. **Erben U, Loddenkemper C**, Doerfel K, et al. A guide to histomorphological evaluation of intestinal inflammation in mouse models. Int J Clin Exp Pathol 2014;7:4557–4576.

23. Neimark E, Chen F, Li X, et al. c-Fos is a critical mediator of inflammatory-mediated repression of the apical sodium-dependent bile acid transporter. Gastroenterology 2006;131:554–567.
24. Zheng Z, Jiang H, Huang Y, et al. Screening of an anti-inflammatory peptide from Hydrophis cyanocinctus and analysis of its activities and mechanism in DSS-induced acute colitis. Sci Rep 2016;6:25672.
25. Chiang JYL, Ferrell JM. Bile acids as metabolic regulators and nutrient sensors. Annu Rev Nutr 2019;39:175–200.
26. Sato T, Vries RG, Snippert HJ, et al. Single Lgr5 stem cells build crypt-villus structures in vitro without a mesenchymal niche. Nature 2009;459:262–265.
27. Zhang Y-KJ, Guo GL, Klaassen CD. Diurnal variations of mouse plasma and hepatic bile acid concentrations as well as expression of biosynthetic enzymes and transporters. PLoS One 2011;6:e16683.
28. Hofmann AF. The continuing importance of bile acids in liver and intestinal disease. Arch Intern Med 1999; 159:2647.
29. Sangiorgi E, Capecchi MR. Bmi1 is expressed in vivo in intestinal stem cells. Nat Genet 2008;40:915–920.
30. Cheng K, Chen Y, Zimniak P, et al. Functional interaction of lithocholic acid conjugates with M3 muscarinic receptors on a human colon cancer cell line. Biochim Biophys Acta 2002;1588:48–55.
31. Abrams P, Andersson K-E, Buccafusco JJ, et al. Muscarinic receptors: their distribution and function in body systems, and the implications for treating overactive bladder. Br J Pharmacol 2006;148:565–578.
32. Lund ML, Sorrentino G, Egerod KL, et al. L-cell differentiation is induced by bile acids through GPBAR1 and paracrine GLP-1 and serotonin signaling. Diabetes 2020; 69:614–623.
33. **Reimann F, Habib AM**, Tolhurst G, et al. Glucose sensing in L cells: a primary cell study. Cell Metab 2008; 8:532–539.
34. Wang B, Rong X, Palladino, et al. Phospholipid remodeling and cholesterol availability regulate intestinal stemness and tumorigenesis. Cell Stem Cell 2018; 22:206–220.e4.
35. Zhao B, Ye X, Yu J, et al. TEAD mediates YAP-dependent gene induction and growth control. Genes Dev 2008;22:1962–1971.
36. Zanconato F, Cordenonsi M, Piccolo S. YAP/TAZ at the roots of cancer. Cancer Cell 2016;29:783–803.
37. Anakk S, Bhosale M, Schmidt VA, et al. Bile acids activate YAP to promote liver carcinogenesis. Cell Rep 2013; 5:1060–1069.
38. Lee C, Jeong S, Jang C, et al. Tumor metastasis to lymph nodes requires YAP-dependent metabolic adaptation. Science 2019;363:644–649.
39. **Serra D, Mayr U, Boni A**, et al. Self-organization and symmetry breaking in intestinal organoid development. Nature 2019;569:66–72.
40. Zanconato F, Forcato M, Battilana G, et al. Genome-wide association between YAP/TAZ/TEAD and AP-1 at enhancers drives oncogenic growth. Nat Cell Biol 2015; 17:1218–1227.
41. **Yui S, Azzolin L**, Maimets M, et al. YAP/TAZ-dependent reprogramming of colonic epithelium links ECM remodeling to tissue regeneration. Cell Stem Cell 2018;22:35–49.e7.
42. **Liu-Chittenden Y, Huang B**, Shim JS, et al. Genetic and pharmacological disruption of the TEAD-YAP complex suppresses the oncogenic activity of YAP. Genes Dev 2012;26:1300–1305.
43. Hu M-M, He W-R, Gao P, et al. Virus-induced accumulation of intracellular bile acids activates the TGR5-β-arrestin-SRC axis to enable innate antiviral immunity. Cell Res 2019;29:193–205.
44. Nagathihalli NS, Beesetty Y, Lee W, et al. Novel mechanistic insights into ectodomain shedding of EGFR ligands amphiregulin and TGF- : impact on gastrointestinal cancers driven by secondary bile acids. Cancer Res 2014;74:2062–2072.
45. Xu W, Doshi A, Lei M, et al. Crystal structures of c-Src reveal features of its autoinhibitory mechanism. Mol Cell 1999;3:629–638.
46. **Li P, Silvis MR, Honaker Y**, et al. αE-catenin inhibits a Src–YAP1 oncogenic module that couples tyrosine kinases and the effector of Hippo signaling pathway. Genes Dev 2016;30:798–811.
47. Araujo J, Logothetis C. Dasatinib: a potent SRC inhibitor in clinical development for the treatment of solid tumors. Cancer Treat Rev 2010;36:492–500.
48. Tao S, Tang D, Morita Y, et al. Wnt activity and basal niche position sensitize intestinal stem and progenitor cells to DNA damage. EMBO J 2017;36:2920–2921.
49. Ayyaz A, Kumar S, Sangiorgi B, et al. Single-cell transcriptomes of the regenerating intestine reveal a revival stem cell. Nature 2019;569:121–125.
50. Gregorieff A, Liu Y, Inanlou MR, et al. Yap-dependent reprogramming of Lgr5+ stem cells drives intestinal regeneration and cancer. Nature 2015;526:715–718.
51. **Sinha SR, Haileselassie Y**, Nguyen LP, et al. Dysbiosis-induced secondary bile acid deficiency promotes intestinal inflammation. Cell Host Microbe 2020;27:659–670.e5.
52. Sundaram GM, Quah S, Sampath P. Cancer: the dark side of wound healing. FEBS J 2018;285:4516–4534.
53. Farhana L, Nangia-Makker P, Arbit E, et al. Bile acid: a potential inducer of colon cancer stem cells. Stem Cell Res Ther 2016;7:181.
54. Fu T, Coulter S, Yoshihara E, et al. FXR regulates intestinal cancer stem cell proliferation. Cell 2019; 176:1098–1112.e18.

Author names in bold designate shared co-first authorship

Received December 10, 2019. Accepted May 25, 2020.

Correspondence
Address correspondence to: Kristina Schoonjans, PhD, Institute of Bioengineering, School of Life Sciences, École Polytechnique Fédeérale de Lausanne, 1015 Lausanne, Switzerland. e-mail: kristina.schoonjans@epfl.ch; fax: +41-21-693-9600.

Acknowledgments
We thank Andréane Fouassier, Sabrina Bichet, Thibaud Clerc, Laure Vogeleisen-Delpech, Fabiana Fraga, the Phenotyping Unit (UDP), the Histology core facility (HCF), the Flow Cytometry Core Facility (FCCF) and

the BioImaging and Optics Platform (BIOP) of EPFL for technical assistance. All summary or representative data generated and supporting the findings of this study are available within the paper. Raw data that support the findings of this study are available on reasonable request.

CRediT Authorship Contributions
Giovanni Sorrentino, Postdoc (Conceptualization: Lead; Data curation: Lead; Formal analysis: Lead; Funding acquisition: Lead; Investigation: Lead; Methodology: Lead; Project administration: Lead; Validation: Lead; Writing – original draft: Lead). Alessia Perino, Postdoc (Methodology: Supporting). Ece Yildiz, PhD student (Investigation: Supporting). Gaby El Alam, PhD student (Resources: Lead). Maroun Bou Sleiman, Postdoc (Resources: Lead). Antimo Gioiello, Dr (Methodology: Supporting). Roberto Pellicciari, Dr (Methodology: Supporting). Kristina Schoonjans, Professor (Conceptualization: Lead; Funding acquisition: Lead; Project administration: Lead; Supervision: Lead; Writing – original draft: Lead).

Conflict of Interest
These authors disclose the following: Roberto Pellicciari is the president and CEO of TES Pharma. Roberto Pellicciari and Antimo Gioiello are cofounders of TES Pharma. The remaining authors disclose no conflicts.

Funding
The work of Kristina Schoonjans was funded by the Swiss National Science Foundation (SNSF N° 310030_189178, Sinergia CRSII5_180317/1), the Kristian Gerhard Jebsen Foundation, and the Ecole Polytechnique Fédérale de Lausanne (EPFL). Giovanni Sorrentino was funded by a postdoctoral FEBS long-term fellowship.

Supplementary Methods

Western Blotting

Samples were lysed in lysis buffer (50 mM Tris [pH 7.4], 150 mM KCl, 1 mM EDTA, 1% NP-40, 5 mM NAM, 1 mM sodium butyrate, protease and phosphatase inhibitors). Proteins were separated by sodium dodecyl sulfate–polyacrylamide gel electrophoresis and transferred onto nitrocellulose or polyvinylidene difluoride membranes. Blocking (30 minutes) and antibody incubations (overnight) were performed in 5% bovine serum albumin in Tris-buffered saline. The following primaries antibodies were used: YAP1 (Santa Cruz Biotechnology, Dallas, TX; sc101199, 1:1000), phospho-YAP1^{Y357} (Abcam, Cambridge, UK; ab62751, 1:1000), vinculin (Abcam, ab129002, 1:1000), SRC (Cell Signaling, Danvers, MA; 2109S, 1:1000), phospho-SRC^{Y418} (ThermoFisher, Waltham, MA; 44-660G, 1:1000).

Immunofluorescence

Organoids were extracted from Matrigel (with Cell Recovery Solution; Corning, Corning, NY) and fixed with 4% paraformaldehyde (PFA) in phosphate-buffered saline (PBS) (20 minutes, room temperature). Organoids in suspension were centrifuged (1000 rpm, 5 minutes) to remove the PFA, washed with ultra-pure water, and pelleted. The organoids were then spread on glass slides and allowed to attach by drying. Attached organoids were rehydrated with PBS and permeabilized with 0.2% Triton X-100 in PBS (1 hour, room temperature) and blocked (1% bovine serum albumin in PBS) for 1 hour. Samples were then incubated overnight with the indicated primary antibodies: E-cadherin (1:100, 24E10; Cell Signaling), YAP (1:50, 4912S; Cell Signaling), phospho-YAP1^{Y357} (1:50, ab62751), phospho-SRC^{Y418} (1:50, 44-660G; ThermoFisher); GFP (1:200, ab6673; Abcam), L-FABP (1:100, sc50380; Santa Cruz), Chromogranin A (1:100, sc-13090; Santa Cruz), Lysozyme (1:100, PAI-29680; ThermoFisher), Glucagon (1:50, sc-544592; Santa Cruz).

Samples were washed with PBS and incubated for 3 hours with secondary antibodies Alexa 488 donkey-α-rabbit, Alexa 568 donkey-α-mouse, Alexa 647 donkey-α-goat (1:1000 in blocking solution; Invitrogen, Carlsbad, CA). Following extensive washing, stained organoids were imaged by confocal (LSM 710; Zeiss, Oberkochen, Germany) mode. DAPI (4′,6-diamidino-2-phenylindole) was used to stain nuclei. Phase contrast images of organoids were acquired using Nikon (Tokyo, Japan) eclipse Ts2 microscope. For tissue samples, sliced tissue was dewaxed and rehydrated, and quenching was performed with 3% H_2O_2 in PBS. Heat-induced epitope retrieval was performed in 10 mM citrate buffer pH 6 at 95°C for 20 minutes.

RNA In Situ Hybridization

RNAscope Multiplex Fluorescent V2 assay (Cat. No. 323110; Bio-techne, Minneapolis, MN) was performed according to manufacturer's protocol on 4-μm paraffin sections, hybridized with the probes Mm-TGR5 (Gpbar1)-C1 (Cat. No. 318451; Bio-techne) combined with Mm-Lgr5-C2 (Cat. No. 312171-C2; Bio-techne), Mm-2Plex POS (Cat. No. 321651; Bio-techne) as positive control and 2Plex NEG (Cat. No. 320751; Bio-techne) as negative control at 40°C for 2 hours and revealed with TSA Opal650 (Cat. No. FP1496001KT; PerkinElmer, Waltham, MA) for C1 and TSA Opal 570 (Cat. No. FP1488001KT; PerkinElmer) for C2. Tissues were counterstained with DAPI and mounted with FluoromountG (Cat. No. 100.01; Bioconcept, Salem, NH).

Diet Information

The chow diet (CD; Harlan 2918) and HFD (TD06414) used in the study are produced from Harlan Laboratories (Indianapolis, IN). CD contains 18.6% protein, 6.2% fat, and 44.2% carbohydrates (by weight) with an energy density of 3.1 kcal/g. HFD contains 23.5% protein, 34.3% fat, and 27.3% carbohydrates (by weight) with an energy density of 5.1 kcal/g.

Histology

Tissues were swiss rolled, fixed with Formal-fixx overnight at 4°C and embedded in paraffin. Four sections were prepared by microtome (Microm HM325, ThermoFisher, Waltham, MA). Hematoxylin and eosin (Hematoxylin QS; Vector, Eosin Y Solution Aqueous; Sigma) and periodic acid–Schiff staining were performed according to the manufacturer's protocols. Crypt and denuded colon area length was determined using ImageJ on images acquired using Olympus (Tokyo, Japan) slide scanner VS120-L100.

Real-Time Quantitative Reverse Transcription PCR (qRT-PCR) for Messenger RNA quantification

RNA was extracted from organoids with RNAqueous Kit (ThermoFisher) and from tissues with RNeasy plus kit (Qiagen, Hilden, Germany) and was transcribed to complementary DNA using QuantiTect Reverse Transcription Kit (Qiagen) following manufacturer's instructions. Expression of selected genes was analyzed using the LightCycler 480 System (Roche) and SYBR Green chemistry. All quantitative polymerase chain reaction (qPCR) results were presented relative to the mean of Glyceraldehyde 3-phosphate dehydrogenase (*Gapdh*) or beta-actin. The average of at least 3 technical repeats was used for each biological data point. Primers used for qPCR are shown in Supplementary Table 1.

Proliferation Assay

Cell proliferation was assessed by EdU assay (Click-iT EdU Alexa Fluor 647) following manufacturer's instructions. Edu was resuspended in PBS and 200 μL of solution was injected intraperitoneally (50 μg per g of mouse weight). CCK was from Anawa (AS-22944). For in vitro studies, EdU was added to the culture medium (10 μM) for 2 hours.

RNA Sequencing Analysis

For each biological replicate, GFP^{hi} cells were isolated by FACS from intestines from 4 pooled *Lgr5-Tg* mice. Approximately 200,000 GFP^{hi} cells were then embedded in Matrigel (20,000 per well in 10 μL Matrigel drop) and after 4 hours were exposed to INT-777 (30 μM) or dimethyl sulfoxide (DMSO) as control. After 12 hours, RNA was extracted (RNAqueous Kit; ThermoFisher) for RNA sequencing analysis. This experiment was repeated 3 times on 3 different days (n = 3 biological replicates). For each sample, 50 million paired-end sequencing reads of length 100 base pairs each were sequenced using BGISEQ-500 platform. The sequence data have been deposited into the GEO (accession number has been requested). *FastQC* was used to verify the quality of the mapping.[1] No low-quality reads were present and no trimming was needed. Alignment was performed against mouse genome (CRCm38 mm10 primary assembly and Ensembl release 95 annotation) using *STAR* (version 2.73a).[2] The obtained STAR gene-counts for each alignment were analyzed for differentially expressed genes using the R package *edgeR* (version 3.24.3) using a generalized-linear model.[3] A threshold of 1 $\log_2$ fold change and *P* value larger than .05 were considered when identifying the differentially expressed genes. A principal component analysis[4,5] of the data revealed the presence of a batch effect with the third batch (day 3) due to day-to-day technical variability. The *RUVSeq* (version 1.16.1)[6] Bioconductor R package was used to correct for the unwanted variation using a set of empirical control genes (all but top 5000 most significantly expressed genes determined from a first-pass differential expression analysis). The *clusterProfiler*[7] (version 3.10.1) and *RcisTarget* (version 1.2.1) packages were then used for gene ontology and transcription factor binding motif enrichment, respectively.

BA Quantification

The BA measurement was done by stable isotope dilution mass spectrometry assay at the Metabolomics Platform of University of Lausanne.

Standards for calibration. Stock solutions of BAs and D5-labeled BAs (at 1 mg/mL) in methanol were used for the preparation of standard mixtures with a final concentration from 2.5 to 10 μg/mL. Calibrators were prepared by serial dilutions with stripped serum (C0-C7). Internal standard (IS) mixture contained 13 deuterium-labeled BAs.

Sample preparation. The fecal powders were obtained by grinding frozen tissue samples with liquid nitrogen using mortar and pestle. Powders were preweighed to ~100 mg each in the lysis tubes. Samples were homogenized in tissue homogenizer (Precellys, Bertin Instruments, Montigny-le-Bretonneux) by the addition of MeOH:H_2O (2:1) with 0.1% FA (1500 μL) and ceramic beads for 2 × 20 seconds at 10,000 rpm. Homogenized extracts were centrifuged for 15 minutes at 14,000*g* at 4°C, and the supernatants were further treated by solid phase extraction (SPE) for phospholipid removal, as described later in this article. Before loading onto SPE plate, the samples, together with the calibrators and QC samples, were spiked with IS mixture and diluted with H_2O containing 0.2% formic acid. All plates were sealed, homogenized by vortexing, and centrifuged for 5 minutes at 2700*g* at 4°C. The mixtures were loaded onto an Oasis HLB μElution (Waters, Milford, MA) plate. Once loaded, the plate was washed with 5% MeOH in H_2O solution (200 μL) and the analytes were eluted with 100% MeOH (100 μL) after 1 minute of incubation. The eluates were collected and dried under nitrogen flow at 25°C. The dried extracts were reconstituted in 100 μL of 30% acetonitrile in H_2O solution before liquid chromatography high-resolution mass spectrometry (LC-HRMS) analyses.

LC-HRMS analysis. BA quantification was performed on a Vanquish Horizon (ThermoFisher Scientific) ultra-high performance liquid chromatography (UHPLC) system coupled to Q Exactive Focus interfaced with a HESI source operating in negative ionization mode. Chromatographic separation was carried out using an Acquity UPLC HSS T3 1.8 μm 2.1 × 100 mm column (Waters, Milford, MA). Mass spectrometry parameters were set to full scan in mass range *m/z* 370-522, mass resolving power = 70,000 full width at half maximum and automatic gain control target = 5e5.

Data processing. Data were processed using TraceFinder 4.1. software (ThermoFisher Scientific). The linearity was evaluated for each BA. Limit of detection was determined with signal-to-noise (S/N) ratio >3; lower limit of quantification was determined with S/N >5 and <20% coefficient of variation. In addition to accurate *m/z* ratio, the retention time (in minutes) was used to distinguish between different isobaric species. Absolute concentrations were calculated using calibration curves and considering the response factor of corresponding IS. Concentrations were reported to sample dry weight (feces).

Supplementary References

1. Andrews S. FASTQC: A Quality Control tool for High Throughput Sequence Data. ScienceOpen Inc, Boston, MA: Babraham Inst, 2015.
2. Dobin A, Davis CA, Schlesinger F, et al. STAR: Ultrafast universal RNA-seq aligner. Bioinformatics 2013;29:15–21.
3. Robinson MD, McCarthy DJ, Smyth GK, edgeR. A Bioconductor package for differential expression analysis of digital gene expression data. Bioinformatics 2009;26:139–140.
4. Lê S, Josse J, Husson F. FactoMineR: An R package for multivariate analysis. J Stat Softw 2008;25:1–18.
5. Ginestet C. ggplot2: Elegant Graphics for Data Analysis. J R Stat Soc Ser A (Statistics Soc) 2011;174:245–246.
6. Risso D, Ngai J, Speed TP, et al. Normalization of RNA-seq data using factor analysis of control genes or samples. Nat Biotechnol 2014;32:896–902.
7. Yu G, Wang LG, Han Y, et al. ClusterProfiler: An R package for comparing biological themes among gene clusters. OMICS 2012;16:284–287.

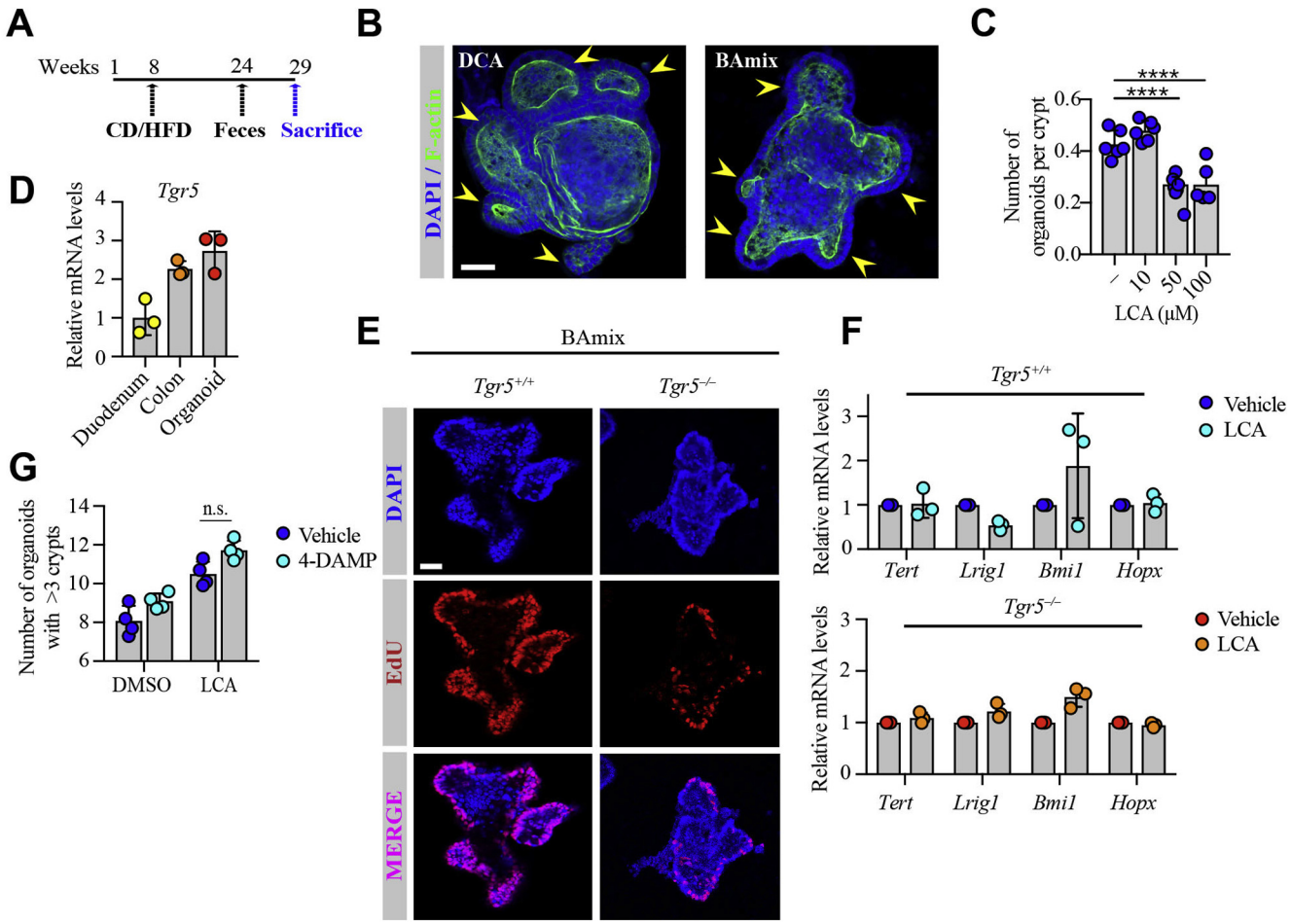

Supplementary Figure 1. (*A*) Workflow of the CD/HFD-feeding experiment. (*B*) Representative picture relative to (*C*). (*C*) Intestinal crypts were isolated from C57BL/6J mice, embedded in Matrigel, and exposed to increasing amount of LCA for 6 days. The efficiency of organoid generation was quantified for statistical analysis (n = 6 biological replicates). (*D*) *Tgr5* expression was analyzed by qRT-PCR in duodenum, colon, or intestinal organoids cultured for 7 days. (*E*) Representative images of EdU incorporation in organoids exposed to BAmix for 6 days. Scale bar (50 μm). (*F*) The expression of the indicated genes was analyzed by qRT-PCR in intestinal organoids from $Tgr5^{+/+}$ and $Tgr5^{-/-}$ mice exposed to LCA (10 μM) for 6 days (n = 3 mice per genotype). (*G*) Intestinal crypts were exposed to LCA (10 μM) alone or with 4-DAMP (10 μM) for 6 days. The organoid buddings were quantified for statistical analysis (n = 4). Graphs represent mean ± SD. *$P < .05$, **$P < .01$, ****$P < .0001$. *P* values were calculated using 1-way analysis of variance (*C*, *D*) or 2-way analysis of variance (*F*, *G*).

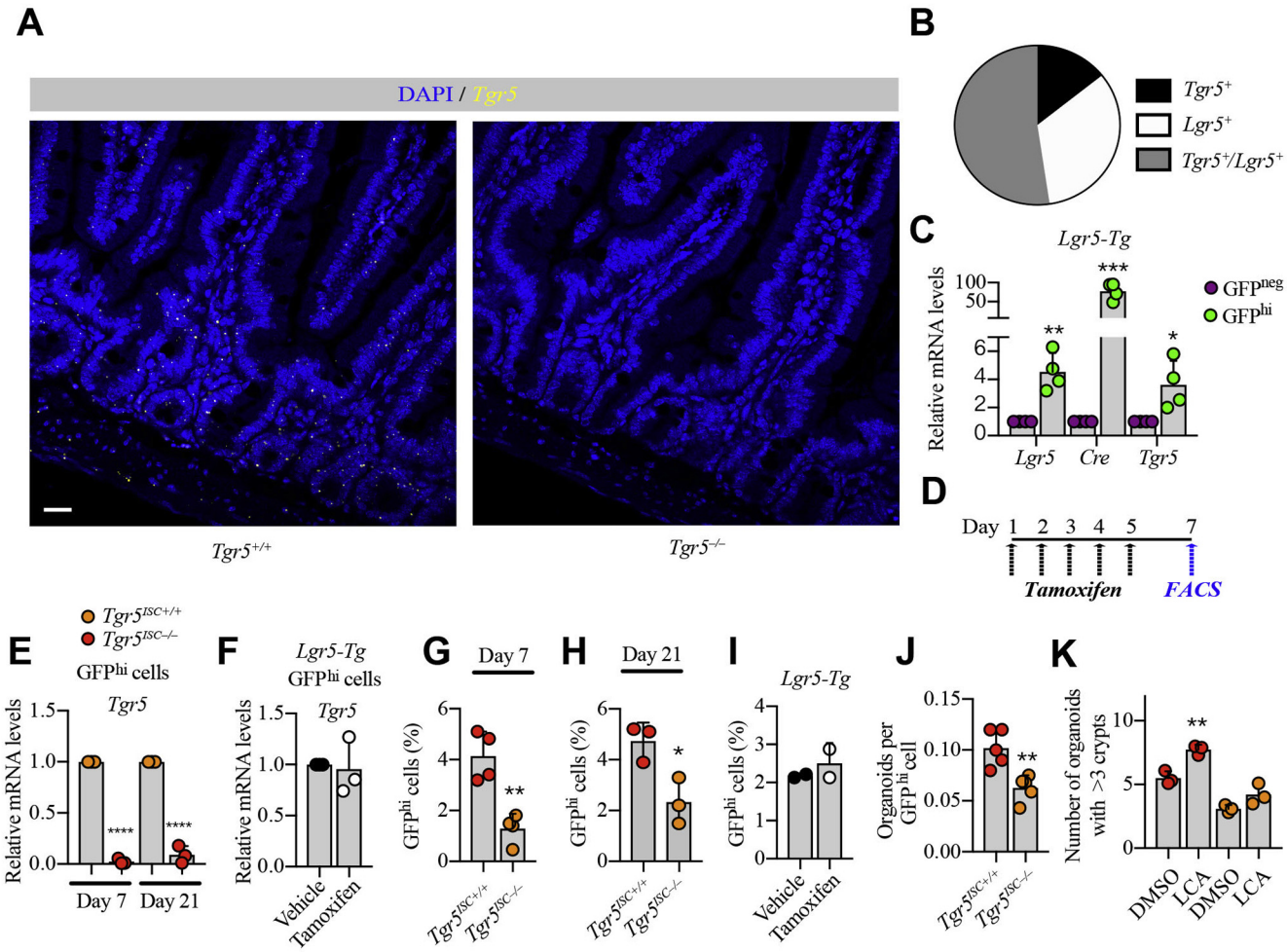

Supplementary Figure 2. (*A*) *Tgr5* (*yellow dots*) in situ hybridization was performed in intestinal sections from $Tgr5^{+/+}$ and $Tgr5^{-/-}$ mice. Scale bar (50 μm). (*B*) Pie chart representing the percentage of $Tgr5^{+}$, $Lgr5^{+}$, and double $Tgr5^{+}/Lgr5^{+}$ cells in intestinal crypts as monitored by in situ hybridization in (*A*). (*C*) qRT-PCR in GFP^{hi} and GFP^{neg} cells sorted by flow cytometry (n = 4 biological replicates). (*D*) Workflow of tamoxifen-driven *Tgr5* deletion in $Lgr5^{+}$ cells. Mice were daily injected with tamoxifen for 5 consecutive days followed by 2-day waiting period. (*E*) qRT-PCR of *Tgr5* in GFP^{hi} cells sorted by flow cytometry from $Tgr5^{ISC+/+}$ *and* $Tgr5^{ISC-/-}$ (n = 3 mice per genotype). (*F*) qRT-PCR of *Tgr5* in GFP^{hi} cells sorted by flow cytometry from vehicle- or tamoxifen-exposed *Lgr5-Tg* mice (n = 3 mice per genotype). (*G* and *H*) Percentage of GFP^{hi} and GFP^{neg} cells in the entire small intestine measured by flow cytometry after 7 (n = 4 mice per genotype) (*G*) or 21 days (n = 3 mice per genotype) (*H*) on last tamoxifen administration. (*I*) Percentage of GFP^{hi} cells in the entire small intestine of *Lgr5-Tg* mice measured by flow cytometry as a control of tamoxifen exposure (n = 2 mice per genotype). (*J*) Quantification of organoid generation efficiency relative to (*G*) (n = 5 mice per genotype). (*K*) Intestinal crypts were isolated and exposed to DMSO or LCA (10 μM) for 6 days. The organoid buddings were quantified for statistical analysis (n = 3). Graphs represent mean ± SD. $^{*}P < .05$, $^{**}P < .01$, $^{***}P < .001$, $^{****}P < .0001$. *P* values were calculated using 1-way analysis of variance or two-tailed Student *t* test (*C*).

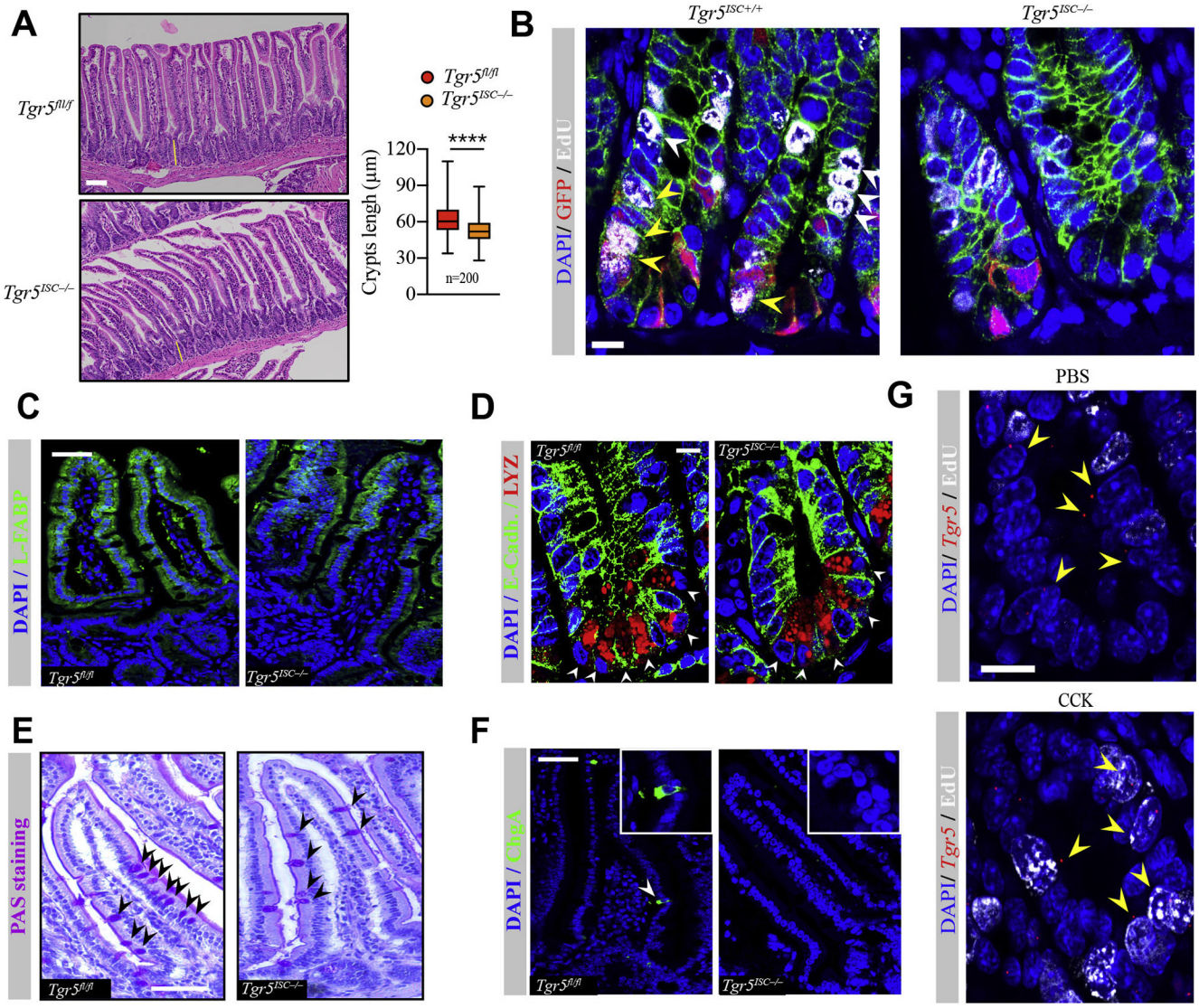

Supplementary Figure 3. (*A*) Representative histology (*left*) and quantification of crypt length (*right*) in mouse jejunum sections from indicated genotypes (n = 200 crypts per group). Scale bar (100 μm). (*B*) Representative pictures showing crypt cell proliferation (by EdU staining) in the stem cell compartment (GFP^+ cells) and progenitor compartment (GFP^- cells). *White arrows* indicate proliferating TA cells, *yellow arrows* indicate proliferating ISC. (*C–F*) Representative pictures relative to (*C*) showing immunofluorescence for L-FABP, Lysozyme and E-cadherin, Chromogranin A and periodic acid–Schiff staining. Scale bars (50 μm: *C*, *E*, *F*; 10 μm: *D*). (*G*) Representative pictures showing *Tgr5*$^+$ cells (indicated with *yellow arrows*) by in situ hybridization and proliferating cells by EdU staining. Graphs represent mean ± SD. ****$P < .0001$. *P* values were calculated using 2-tailed Student *t* test.

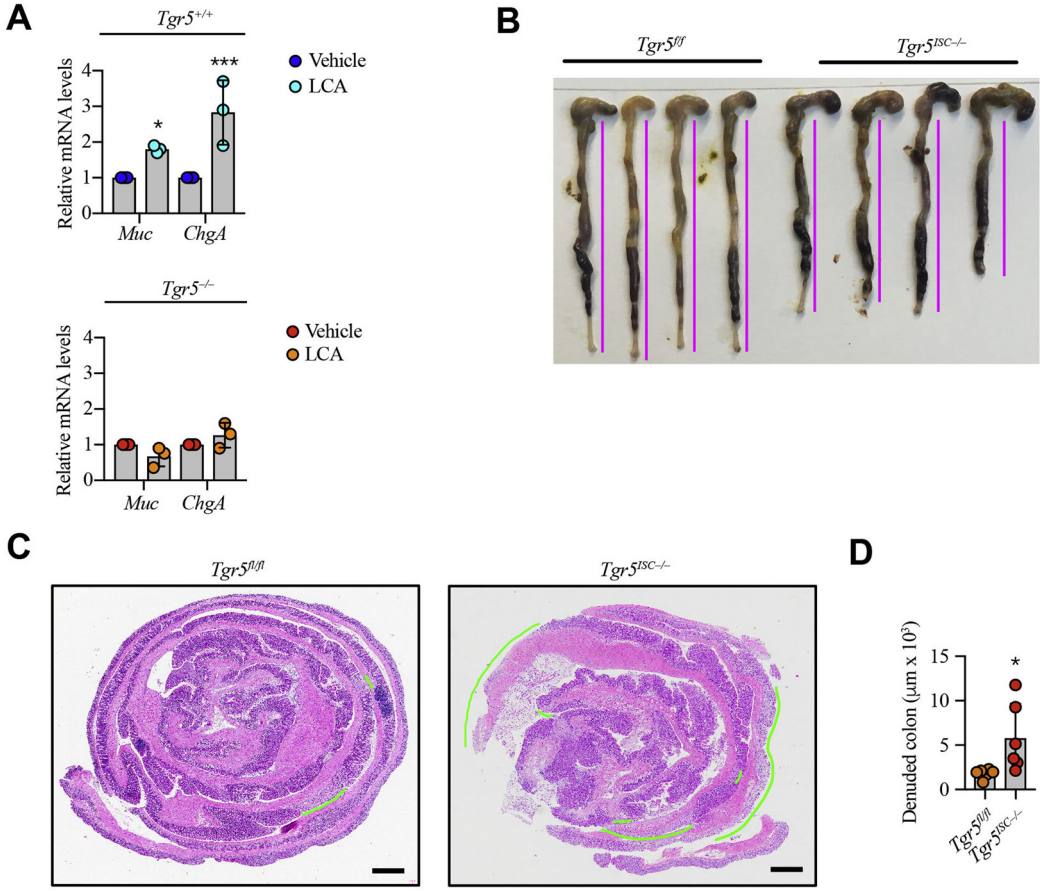

Supplementary Figure 4. (*A*) The expression of the indicated genes was analyzed by qRT-PCR in intestinal organoids from *Tgr5*$^{+/+}$ and *Tgr5*$^{-/-}$ mice exposed to LCA (10 μM) for 6 days (n = 3 mice per genotype). (*B*) Colons from mice of the indicated genotypes 7 days after DSS initiation, relative to (*A–C*) (n = 4). (*C*) Representative hematoxylin-eosin staining of Swiss roll-colon from DSS-exposed mice (day 7). *Green lines* indicate ulceration area. Scale bar (1 mm). (*D*) Quantification of the length of the denuded area in colon from DSS-exposed mice (day 7). Graphs represent mean ± SD. **P* < .05, ****P* < .001. *P* value is calculated using 2-tailed Student *t* test.

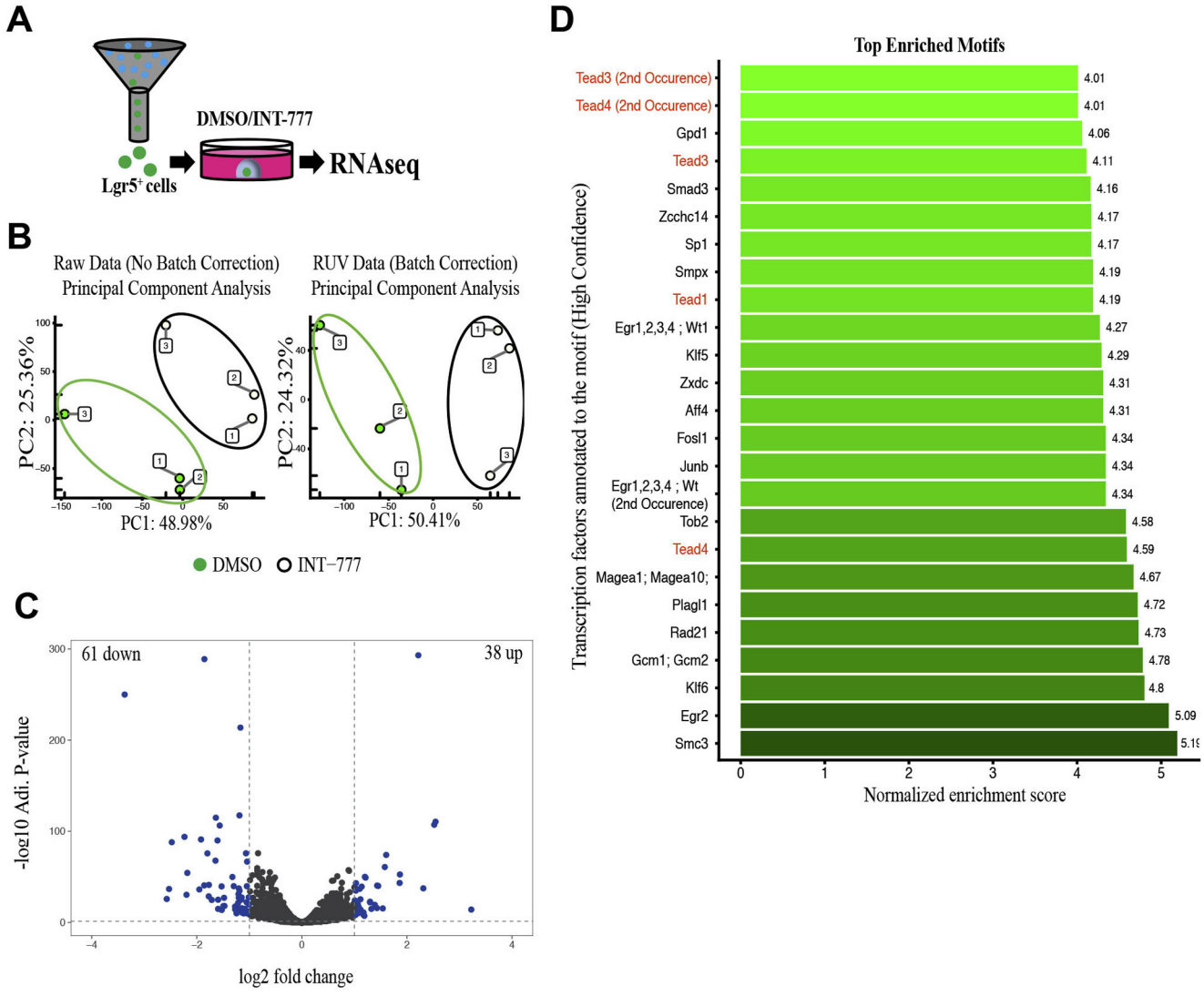

Supplementary Figure 5. (*A*) Scheme of RNA sequencing (RNAseq) workflow. For each biological replicate, GFP^{hi} cells were isolated from intestines from 4 pooled Lgr5-Tg mice. GFP^{hi} cells were then embedded in Matrigel and after 4 hours were exposed to INT-777 (30 μM) or DMSO as control. After 12 hours, RNA was extracted for RNAseq analysis. This experiment was repeated 3 times in 3 different days (n = 3 biological replicates). (*B*) Plot for principal component analysis (*left*) before any batch correction (raw counts following TMM normalization and basic filtering only) and (*right*) following batch correction using RUV-seq R package. A clear batch effect can be observed (*left*) due to day-to-day technical variability. However, following correction, the 2 groups (DMSO and INT-777) cluster into 2 distinct groups (*right*). (*C*) Volcano plot of log2 fold change vs −log10 of the *P* value after batch correction. The number of upregulated and downregulated genes are highlighted. (*D*) Barplot of the top 25 high confidence most enriched motifs (based on normalized enrichment score). The family of transcription factors Teads (in *red*) shows high enrichment (as demonstrated by 5 occurrences).

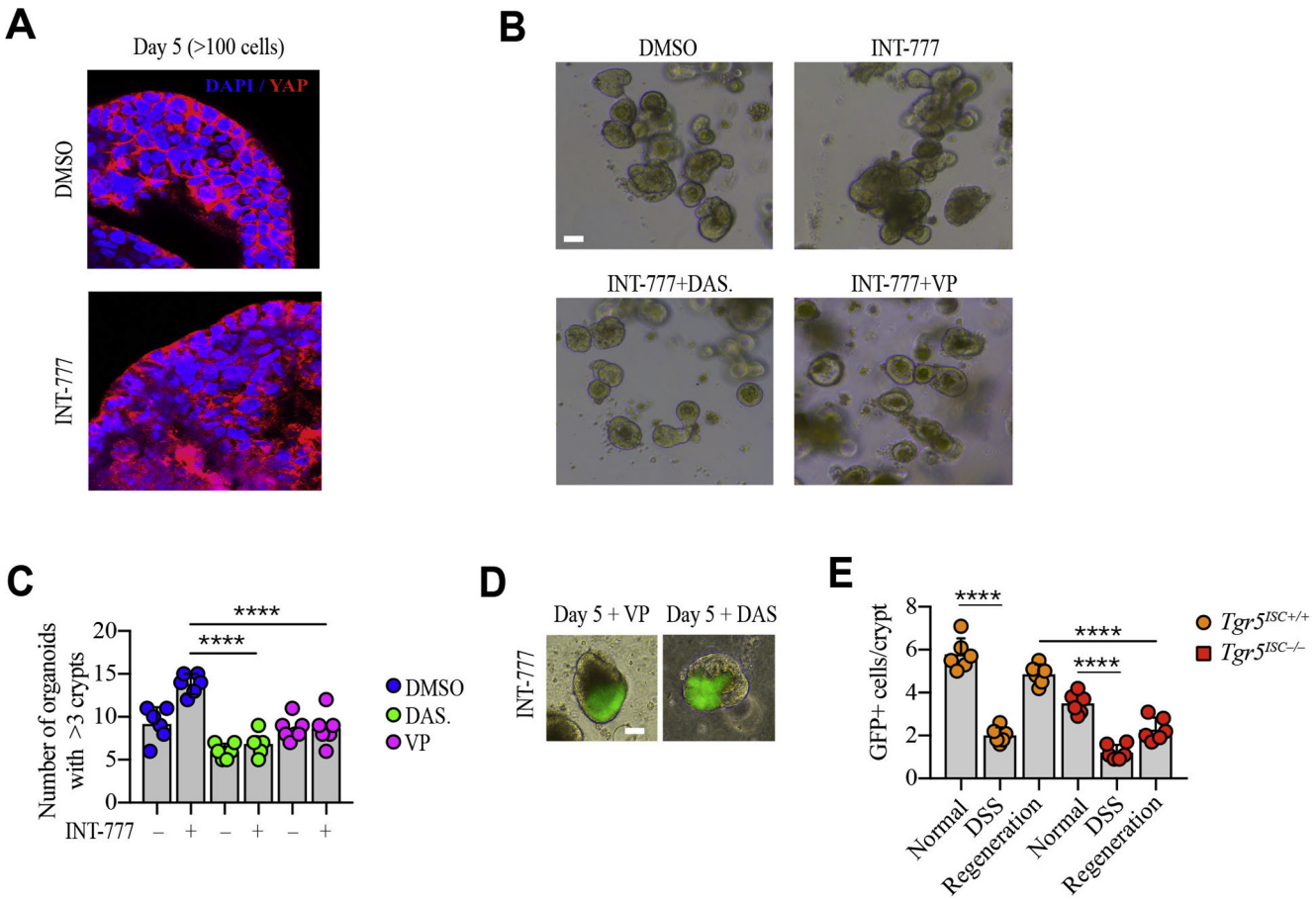

Supplementary Figure 6. (*A*) YAP localization in organoids generated from single GFP^{hi} cells and exposed to DMSO or INT-777 (30 μM) for indicated time. (*B*, *C*) Representative brightfield images (*B*) and quantification (*C*) relative to Figure 5*C*. Scale bar (50 μm). (*D*) Brightfield/epifluorescent image overlay of organoids generated from single isolated GFP^{hi} cells at indicated time points. Verteporfin (VP, 1 μM) and Dasatinib (DAS, 50 nM) were added from day 3 to day 5. Scale bar (10 μm). (*E*) Quantification of GFP^{+} cells in *Lgr5-Tg* crypts from colon samples from mice of indicated genotypes either left untreated (Normal), exposed to DSS for 7 days (DSS) or exposed to DSS for 7 days and then allowed to recover for 3 days (Regeneration). Graphs represent mean ± SD. ****$P < .0001$. *P* values were calculated using 1-way analysis of variance.

Supplementary Table 1. List of Primers Used for Quantitative Polymerase Chain Reaction Analysis

Gene	Forward	Reverse
Cyr61	CTGCGCTAAACAACTCAACGA	GCAGATCCCTTTCAGAGCGG
Ctgf	GCTTGGCGATTTTAGGTGTC	CAGACTGGAGAAGCAGAGCC
Axl	ATGGCCGACATTGCCAGTG	CGGTAGTAATCCCCGTTGTAGA
Ankrd1	GCTGGTAACAGGCAAAAAGAAC	CCTCTCGCAGTTTCTCGCT
Areg	AGGGGACTACGACTACTCAG	GAAACTTGGCAGTGCATGGA
Ereg	TGCTTTGTCTAGGTTCCCACC	GGCGGTACAGTTATCCTCGG
Anxa1	AAGGTGGTCCTGGGTCAGC	TGAGCATTGGTCCTCTTGGT
Trop2	TCAACCACTCTGACCTAGACT	TGCCGAAGCTCTATCTGAATG
Ly6f	AGAGGAAGTAAGGACTGGTGT	GCTCTTTCTGCACACAATAGGA
Lgr5	ATTCGGTGCATTTAGCTTGG	CGAACACCTGCGTGAATATG
Gapdh	GGAGAGTGTTTCCTCGTCCC	ACTGTGCCGTTGAATTTGCC
Cre	CGTACTGACGGTGGGAGAAT	CCCGGCAAAACAGGTAGTTA
Tgr5	TCCTGTCAGTCTTGGCCTATGA	GGTGCTGCCCAATGAGATG
Tert	AGCGGGATGGGTTGCTTTTAC	CACCCATACTCAGGAACGCC
Lrig1	AAGGGAACTCAACTTGGCGAG	ACGTGAGGCCTTCAATCAGC
Bmi1	GGAGAAGAAATGGCCCACTACC	TTGGCCTTGTCACTCCCAGA
Hopx	CATCCTTAGTCAGACGCGCA	AGGCAAGCCTTCTGACCGC
Muc2	CCGACTTCAACCCAAGTGAT	GAGCAAGGGACTCTGGTCTG
ChgA	AAGGTGATGAAGTGCGTCCT	GGTGTCGCAGGATAGAGAGG
Beta-actin	GAGACCTTCAACACCCC	GTGGTGGTGAAGCTGTAGCC